



Effect of leaching on the composition of hydration phases during chloride exposure of mortar

Alisa Machner^{a,b,*}, Marie H. Bjørndal^a, Harald Justnes^c, Lucija Hanžič^d, Aljoša Šajna^d, Yushan Gu^e, Benoît Bary^e, Mohsen Ben Haha^f, Mette R. Geiker^a, Klaartje De Weerd^a

^a Norwegian University of Science and Technology, NTNU, Department of Structural Engineering, Richard Birkelandsvei 1A, 7491 Trondheim, Norway

^b Technical University of Munich, TUM School of Engineering and Design, Department of Materials Engineering, Professorship for Mineral Construction Materials, Franz-Langinger-Straße 10, 81245 Munich, Germany

^c SINTEF Building and Infrastructure, Strindvegen 4, 7045 Trondheim, Norway

^d Slovenian National Building and Civil Engineering Institute, Dimičeva 12, 1000 Ljubljana, Slovenia

^e Université Paris-Saclay, CEA, Service d'Etude du Comportement des Radionucléides, 91191 Gif-sur-Yvette, France

^f Heidelberg Technology Center, Oberklamweg 6, 69181 Leimen, Germany

ARTICLE INFO

Keywords:

Chloride binding
Friedel's salt
Kuzel's salt
pH
GEMS
Thermodynamic modelling

ABSTRACT

Mortar specimens were exposed to either a 3% NaCl solution or a 3% NaCl+KOH solution for up to 180 days. Exposure to the NaCl solution provoked much more leaching than the NaCl+KOH exposure. Leaching strongly impacted the chloride ingress profiles. The extended leaching led to a maximum total chloride content almost three times higher and a deeper chloride penetration than exposure with limited leaching after 180 days. The higher maximum chloride content seems to be linked to the enhanced binding capacity of the C-S-H and AFm phases upon moderate leaching as determined by SEM-EDS. The total chloride profile appears to be governed by multi-ion transport and the interaction of chloride with the hydration phases. Service life prediction and performance testing both rely on total chloride profiles and therefore ought to take these interactions into account.

1. Introduction

Reinforced concrete is a commonly used construction material for infrastructure exposed to sea water or de-icing salts, such as harbours, tunnels and bridges. One of the main degradation mechanisms for these reinforced concrete structures is chloride-induced corrosion of the steel reinforcement. The design life of these structures is therefore often determined by the time it takes for chlorides to penetrate through the concrete cover and reach a critical chloride content at the steel surface, which enables pitting corrosion of the reinforcement steel.

1.1. Total chloride profiles

To determine how far chlorides have penetrated into the concrete, chloride ingress profiles are obtained. These profiles give the total chloride content in the concrete as a function of depth below the exposed surface. Such total chloride profiles can be obtained from both existing structures to predict their remaining service life, and from laboratory-

exposed specimens to predict the durability performance of a given cement or concrete.

For engineering purposes, chloride ingress is often predicted using Fick's 2nd law, which considers non-steady-state diffusion as the governing transport mechanism [1,2]. The validity of using Fick's 2nd law of diffusion as a model has been debated previously [3,4]. The apparent diffusion coefficient and surface concentration are determined by fitting the error function solution of Fick's 2nd law to measured total chloride profiles. The *fib* [1] deals with the potential impact of convection in concrete exposed to drying and wetting, which causes rapid ingress and accumulation of chloride in the outer surface, by subtracting a so-called convection zone from the cover depth. A seeming time dependency of the apparent diffusion coefficient is handled using a so-called ageing exponent, while an observed time dependency of the surface concentration is neglected. By applying the error function solution of Fick's 2nd law, one fails to take into account the interaction between the solids and the sea water or de-icing salts, among other things. In this study, we will show that chloride profiles are strongly dependent on the exposure

* Corresponding author at: Norwegian University of Science and Technology, NTNU, Department of Structural Engineering, Richard Birkelandsvei 1A, 7491 Trondheim, Norway.

E-mail address: alisa.machner@tum.de (A. Machner).

<https://doi.org/10.1016/j.cemconres.2021.106691>

Received 17 September 2021; Received in revised form 7 December 2021; Accepted 11 December 2021

Available online 13 January 2022

0008-8846/© 2022 The Authors. Published by Elsevier Ltd. This is an open access article under the CC BY license (<http://creativecommons.org/licenses/by/4.0/>).

conditions and the interaction between the chlorides and solids, which should therefore be taken into account in more mechanistic chloride ingress models.

When considering the total chloride profiles, one should note that only a small part of the total chloride content in concrete is present as free chlorides dissolved in the pore solution [5,6]. Most of the chlorides are bound chlorides, which are either chemically bound in chloride-containing AFm phases or physically bound by the C-S-H.

1.2. Cl-binding in AFm

The two main chloride-containing AFm phases are Friedel's salt ($3\text{CaO}\cdot\text{Al}_2\text{O}_3\cdot\text{CaCl}_2\cdot 10\text{H}_2\text{O}$) and Kuzel's salt ($3\text{CaO}\cdot\text{Al}_2\text{O}_3\cdot 0.5\text{CaSO}_4\cdot 0.5\text{CaCl}_2\cdot 11\text{H}_2\text{O}$). A solid solution with Friedel's salt and monocarbonate or hydroxy AFm as end members has also been reported previously [7–12]. The chloride content of this solid solution depends on the chloride concentration and the pH in the solution [7,13]. Kuzel's salt, however, has been observed to be unstable in the presence of even small amounts of carbonate [7]. Moreover, only limited solid solutions of Kuzel's salt and either monosulphate or Friedel's salt have been reported [7].

1.3. Cl-binding in C-S-H

In addition to chemical binding in AFm phases, chlorides can also be bound physically by accumulating in the diffuse layer of the C-S-H as explained by the electric double layer theory [14]. The physical binding of chlorides in C-S-H for example can be demonstrated by comparing hydrated cement paste exposed to CaCl_2 and NaCl solutions. The chloride binding in cement paste exposed to CaCl_2 can be as much as three times greater than in paste exposed to NaCl solutions with the same chloride concentration [15–22]. Part of the increase observed for exposure to CaCl_2 may be due to increased chloride binding in AFm, but a large part can be attributed to physical binding in C-S-H [17]. CaCl_2 leads to an increase in the calcium concentration and a decrease in the pH of the pore solution [15–22]. The increase in the calcium concentration causes the originally negative surface charge of the C-S-H to be overcompensated by the accumulation of divalent calcium ions in the Stern layer of the C-S-H, turning its charge positive [23]. This, in addition to the reduced competition with the hydroxyl ions [24] due to the lowering of the pH, results in the accumulation of chloride anions in the diffuse layer of the C-S-H, which explains the much greater chloride binding in hydrated cement paste exposed to CaCl_2 than in paste exposed to NaCl [20].

It should be noted that compounds forming between calcium chloride and calcium hydroxide, such as $\text{CaCl}_2\cdot 3\text{Ca}(\text{OH})_2\cdot 12\text{H}_2\text{O}$ and $\text{CaCl}_2\cdot \text{Ca}(\text{OH})_2\cdot \text{H}_2\text{O}$, might also contribute to the chloride uptake in solids [25–29].

1.4. Impact of exposure

In previous laboratory and field studies on mortar and concrete specimens exposed to chloride ingress by diffusion, we observed a correlation between the total chloride profiles and the extent of leaching determined with portlandite or potassium profiles [6,30]. Extended leaching at the exposed surface of the mortar and concrete specimens led to a reduced total chloride content at the exposed surface. Slightly deeper into the specimen, moderate leaching seemed to lead to an increase in the total chloride content. Since most of the chlorides are bound, our hypothesis is that these observed changes in the total chloride content upon leaching are related to changes in chloride-binding capacity.

To investigate the impact of leaching on chloride binding, a closed system experimental set-up was used in recent studies [13,31]. Finely ground hydrated cement paste was left to equilibrate with a range of chloride-containing exposure solutions in which the pH was adjusted

with HCl to simulate leaching [13,31]. It was shown that, when the pH in the exposure solution decreased from approx. 13.5 to approx. 12, the chloride-binding of the cement paste more than doubled [13,31]. This observation bears similarity to the exposure to CaCl_2 mentioned earlier [15–20]. On the one hand, the increased chloride binding was attributed to an increase in the amount and a change in the composition of the AFm phases [13,32]. It was shown that, with the pH decreasing from 13.5 to approx. 12, the Cl/Al ratio in the AFm phases increased from approx. 0.4 to the ideal composition of Friedel's salt, which has a Cl/Al ratio of 1. On the other hand, decreasing pH also enhances the physical binding of chlorides by C-S-H, because there is less competition with hydroxyl ions for the accumulation in the diffuse layer of the C-S-H phase [33] and the surface charge of the C-S-H is more positive due to leaching [34]. Moreover, it was shown that, when the pH drops below 11, the amount of chloride bound by the cement paste decreases due to the dissolution of the chloride-binding hydration phases [13]. At pH levels around 9.5, chloride binding in the paste dropped to negligible levels. These findings indicate that leaching has a major impact on chloride binding and can therefore strongly affect the total chloride profiles.

1.5. Experimental approach in this study

To demonstrate the impact of leaching on chloride ingress profiles, we designed an experimental laboratory set-up for chloride ingress in mortar by diffusion, using two exposure solutions with different pH values and thus creating different leaching conditions.

For the mortar specimens which were to be exposed to severe leaching conditions, we chose a 3% NaCl solution in compliance with a standard performance test for chloride resistance of concrete, such as EN 12390-11 [35]. The pure NaCl solution was expected to show a pH value of around 7. The neutral pH of the NaCl solution would contrast with the high pH of the pore solution of the mortar specimens and cause leaching of among others calcium and alkalis such as potassium as well as hydroxyl anions from the exposed specimens into the exposure solution during the time of exposure. To enhance the leaching even more, the exposure solution was replaced weekly with a freshly made solution.

Parallel mortar specimens were exposed to a solution with the same chloride concentration but chosen to minimize leaching. The best way to limit leaching during exposure is to mimic the pore solution composition in the exposure solution composition. In other words, the exposure solution should have a high pH and contain calcium, alkalis, and other elements in similar concentrations to those in the pore solution of the cement paste. Instead of recreating the entire complex pore solution, we simplified matters by adding KOH to the NaCl exposure solution to match the potassium concentration of the pore solution of a cement paste. In the rest of this paper, we will refer to this exposure solution as $\text{NaCl}+\text{KOH}$. It has the same chloride concentration as the NaCl exposure solution, but limits the leaching of potassium from the specimens. The added KOH also raises the pH of the exposure solution to approx. 13.2. This high pH in the exposure solution limits the solubility of calcium and therefore also limits the leaching of calcium from the specimens. The $\text{NaCl}+\text{KOH}$ solution was also replaced every week to maintain the same chloride load as with the NaCl exposure.

In a previous study [36] using the same exposure set-up and similar specimens, leaching was observed to have a strong impact on the total chloride profiles after half a year of exposure. The maximum total chloride content of the specimens with limited leaching was approx. 1/3 of the maximum in the parallel specimens exposed to a pure NaCl solution, and the chloride ingress depth was reduced by approx. 40% [36]. This showed that the pH of the exposure solution, i.e., the leaching conditions during the exposure, had played a significant role in determining the shape of the total chloride profile and consequently the apparent chloride resistance [36].

In the current study, our aim was to link the changes in the total chloride profiles with changes in the hydration phases. We wanted to find out whether the chloride binding in the diffusion-exposed mortar

specimens would show a similar pH dependency as those observed by Hemstad et al. in the closed simplified systems on cement paste [13].

Total chloride profiles were obtained from mortar specimens exposed to the two solutions, NaCl and NaCl+KOH. Portlandite and potassium profiles were determined from the same specimens as indicators for the degree of leaching. This would enable us to establish a correlation between chloride ingress and leaching depth. In addition, polished sections from the outermost 3 cm from the exposed surface of the mortar specimens were investigated with SEM-EDS to obtain information on their C-S-H and AFm composition and any changes in composition as a function of depth below the exposed surface. Our hypothesis was that the shape of the total chloride profiles would be strongly affected by the interaction between the chlorides and the solids, i.e., the chloride binding. We also provide an outlook on how these findings would affect service life prediction models and the testing of concrete in reinforced concrete structures exposed to chloride ingress.

2. Materials and methods

2.1. Materials

In this study, we used a novel composite cement developed and supplied by HeidelbergCement, in which 43 wt% of the Portland cement is replaced with ground granulated blast furnace slag (GGBFS) and 10 wt % with fly ash (FA). This composite cement is not included in the current version of the EN 197-1 [37], but falls into the category of a CEM VI (S-V) in the recently released non-harmonized version of EN 197-5 [38]. The chemical composition of the cement, as determined with XRF, is given in Table 1.

2.2. Preparation and exposure of the mortar specimens

From this composite cement, mortar cylinders were cast in accordance with EN 12390-2 [39] and prepared for exposure in accordance with EN 12390-11 [35]. The mortar mix design used in this study was developed by HeidelbergCement and Acciona and is given in Table 2.

The mortars were mixed in a planetary concrete mixer (Galletti P50) in batches of 40 L in accordance with the following procedure: all solid components were mixed for 20 s at 30 rpm; approximately $\frac{3}{4}$ of the mixing water was then added, followed by mixing for 60 s at 59 rpm; finally, the remaining mixing water and admixtures were added, followed by mixing for another 10 min at 59 rpm. The admixtures used in this study were added in order to achieve an S5 consistency according to EN 206 in the fresh state [40].

The mortar mixes were cast into cylindrical moulds with a nominal height of 20 cm and a nominal diameter of 10 cm. The filled moulds

Table 1

Chemical composition of the novel composite cement CEM VI (S-V) used in this study as determined by XRF [wt%]. The CEM VI (S-V) cement was developed by HeidelbergCement as part of the EnDurCrete project.

Oxide	[wt%]
SiO ₂	31.79
Al ₂ O ₃	8.36
TiO ₂	0.37
MnO	0.09
Fe ₂ O ₃	2.05
CaO	48.72
MgO	3.56
K ₂ O	0.9
Na ₂ O	0.29
SO ₃	2.43
P ₂ O ₅	0.09
LOI	0.79
Total (1050 °C)	99.44

Table 2

Mortar mix design used in this study in [kg/m³].

		Mass of components [kg/m ³]
Cement	CEM VI (S-V)	561.6
Aggregates	Sand (0–4)	1510
Admixtures	Sika ViscoCrete ^a	1.6
	Sika ViscoFlow ^b	2.3
Water		241
w/c ratio		0.43

^a PCE-based superplasticizer.

^b Workability-retaining admixture.

were covered with plastic foil and stored in the laboratory. After 1 day, the specimens were demoulded and stored at 20 °C at 95% RH for 21 days. After 21 days, the specimens were sealed with plastic foil and kept at 20 °C for further curing. The specimens were cured for 76 days to ensure a sufficiently high degree of reaction of the supplementary cementitious materials in the composite cement, i.e. GGBFS and FA.

After 76 days of curing, a test specimen with a nominal height of approx. 75 mm was sawn from each cylinder (see Fig. 1). After cutting, all the test specimens were vacuum-saturated with deionized water at approx. 2 mbar in a 100 L tank. Max. 24 h after the vacuum saturation, the test specimens were dried under laboratory conditions until the surfaces appeared dry (approx. 6 h), and all surfaces except the sawn surface were coated with epoxy. The epoxy was dried under laboratory conditions overnight. The sealed specimens were then immersed in 2 L of a calcium hydroxide saturated solution for 18 h to facilitate saturation before exposure.

Two exposure solutions were prepared: a 3% NaCl solution and a 3% NaCl+KOH solution. The 3% NaCl solution was prepared by adding 30 g of laboratory-grade NaCl to 970 g of deionized water in accordance with EN 12390-11 [35]. The 3% NaCl+KOH solution was prepared by dissolving 8.416 g of laboratory-grade KOH in 1000 g of deionized water, which is equivalent to a 150 mmol/L KOH concentration. Then, 30 g of laboratory-grade NaCl was added to 970 g of the KOH solution. It should be noted that the KOH concentration was based on a preliminary estimation of the potassium concentration in the pore solution of the hydrated cement using thermodynamic modelling.

For each exposure time and each exposure solution, a set of twin test specimens were prepared. The exposure set-up for a set of twin test specimens in each exposure solution is schematically illustrated in Fig. 2. Half of the sealed and saturated test specimens were immersed in the NaCl solution and half were immersed in the NaCl+KOH solution. The boxes containing the immersed test specimens were closed to prevent evaporation of the exposure solution. The exposure solutions for all test specimens were replaced weekly with fresh exposure solution. For all specimens, the same surface-to-exposure solution volume was applied (13 mL/cm²), which was kept constant over the whole period of exposure.

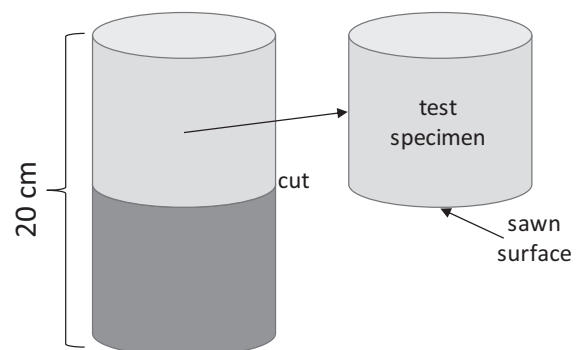


Fig. 1. Sawing the test specimens from each mortar cylinder.

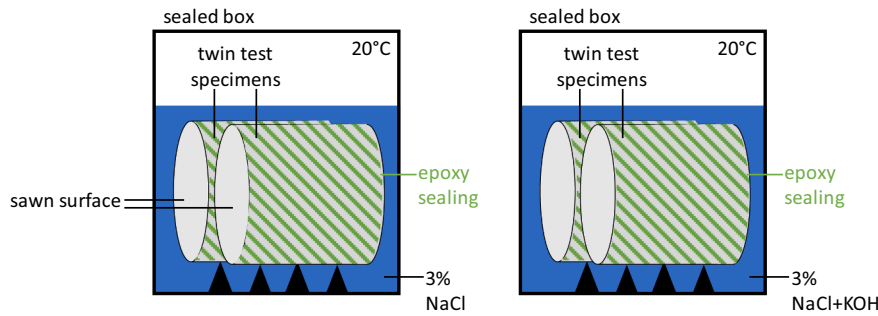


Fig. 2. Exposure of the mortar test specimens to the 3% NaCl solution (left) or the 3% NaCl+KOH solution (right).

2.3. Analyses after exposure

At each testing time, i.e., after 90 and 180 days of exposure, two twin test specimens were taken out of each exposure solution for the preparation for the various analyses after exposure.

One of each twin test specimens was profile-ground from its exposed surface inwards as shown in Fig. 3. The powder samples obtained from various depths below the exposed surface were used to determine the portlandite content in each layer by thermogravimetric analysis (TGA), to determine their total chloride content by potentiometric titration, and to determine their acid-soluble chemical composition by inductively coupled plasma mass spectrometry (ICP-MS).

For TGA, a Mettler Toledo TG/DSC 3+ was used. Approx. 300 mg of each powder sample was poured into 600 µL corundum crucibles. The weight of the samples was measured, while they were heated from 40 to 900 °C at a heating rate of 10 °C/min. During the measurements, the measurement cell was purged with 50 mL N₂/min.

The portlandite (CH) content in each sample was determined by the weight loss between approx. 400 °C (*w*₄₀₀) and 550 °C (*w*₅₅₀) by integrating the derivative weight loss curve and multiplying it by the molar mass ratio of portlandite (74 g/mol) and water (18 g/mol), as proposed by Lothenbach et al. [41]. The portlandite content was then normalized to the dry mortar weight at 550 °C, as shown in Eq. (1), and plotted as a function of depth below the exposed surface. It should be noted that the results for samples in which the carbonate weight loss started before 550 °C were normalized to the sample weight at the temperature just before decomposition of the carbonates started.

$$CH_{dry} = \frac{w_{400} - w_{550}}{w_{550}} \times \frac{74}{18} \tag{1}$$

The weight loss in the range of approx. 250 °C (*w*₂₅₀) to 400 °C (*w*₄₀₀) related to the decomposition of AFm was determined by integration [32] and normalized to the dry mortar weight at 550 °C, as shown in Eq. (2). In contrast to the quantification of the portlandite, no quantification of

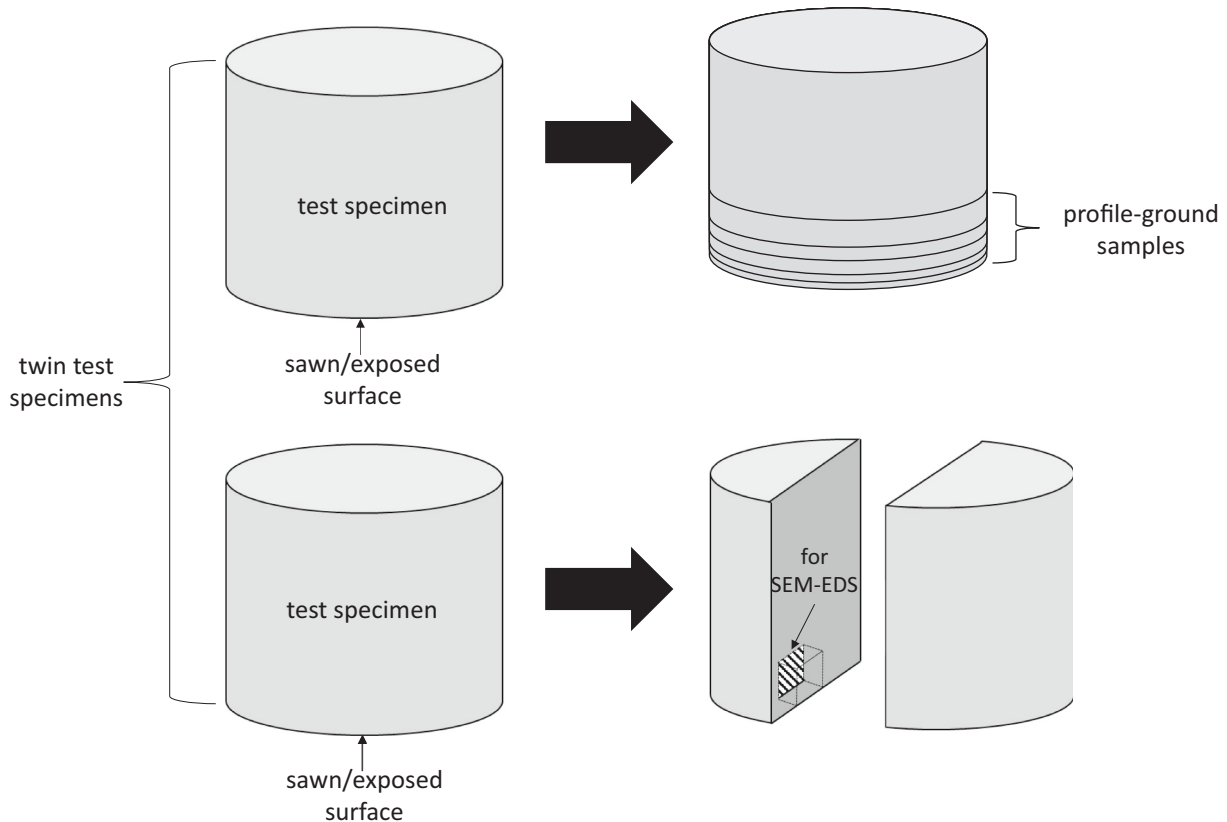


Fig. 3. Illustration of the position of the sampling by profile-grinding for subsequent chemical analysis (top) and of the samples cut for SEM-EDS analysis (bottom) in each set of test specimens.

the specific AFm phases was performed. This was because the composition of the AFm phases was expected to vary within the samples, so that their molar mass and crystalline water content would also vary. The results are therefore semi-quantitatively presented as a weight loss within the relevant temperature interval.

$$wt.\text{LOSS}_{AFm,dry} = \frac{W_{250} - W_{400}}{W_{550}} \quad (2)$$

It should be noted that, when studying leaching, the mass at 550 °C is not constant because portlandite (and probably other hydration phases) will dissolve during leaching, resulting in an overall loss of material. An earlier study [42] made a correction for this loss of material due to leaching. However, in this study we did not, because normalization to 550 °C is conservative when studying a decrease in a specific phase since a certain percentage of material loss will lead to a relative enrichment of the remaining phases in the leached sample. As a result, we might slightly underestimate the decrease in portlandite and thereby the extent of leaching, causing us also to slightly overestimate the amount of AFm phase in the leached sections.

The portlandite content and weight loss due to AFm decomposition were determined as one single measurement for each of the powders obtained from the various depths. Consequently, no margin of error was determined for these results. However, the reproducibility of these quantifications is indicated by the variation in the results obtained from the unaffected sections at greater depths in each sample.

It was not possible to determine carbonate (e.g., CaCO₃) profiles with TGA in this study, because the aggregates used in the mortar mixes contained carbonates.

For the determination of the total chloride content and for the ICP-MS analyses, 5.00 (+/- 0.01) g of each profile ground powder sample was weighed in a glass beaker and dried overnight in an aerated oven at 105 °C. After cooling the samples to room temperature in a desiccator, they were weighed again and were dissolved in 80 °C warm HNO₃ (65%, diluted 1:10). After 1 h, the dissolved samples were filtered through a cellulose syringe filter and filled into two 15 mL centrifuge tubes.

For the determination of the total chloride content in each profile ground powder sample, 1–10 mL (depending on the chloride content) of the dissolved and filtered solutions were titrated against a 0.01 mol/L AgNO₃ solution with a Metrohm 905 Titrando. The results of the total chloride content are given [wt%/g mortar dried at 105 °C] as calculated with Eq. (3):

$$Cl \text{ content} = \frac{V_{AgNO_3} \cdot c_{AgNO_3} \cdot M(Cl) \cdot V_{HNO_3} \cdot 0.001}{V_{sample} \cdot m_{mortar,105^\circ C}} \cdot 100\% \quad (3)$$

where V_{AgNO_3} is the volume of silver nitrate added at the inflection point of the titration in [mL], c_{AgNO_3} is the concentration of the silver nitrate solution (0.01 mol/L), $M(Cl)$ is the molar mass of chlorine (35.453 g/mol), V_{HNO_3} is the volume of diluted nitric acid used to dissolve the ground mortar samples (50 mL), V_{sample} is the volume of dissolved and filtered solution used for the titration (1–10 mL depending on the chloride content), and $m_{mortar,105^\circ C}$ is the mass [g] of the ground mortar samples after drying at 105 °C. The margin of error was not determined for the chloride content in this study. The standard deviation reported on similar experiments by De Weerd et al. [30] of 0.03 wt%/g mortar dried at 105 °C was therefore used as an indication of the margin of error.

For the ICP-MS measurements, the dissolved and filtered solutions were diluted approx. 1:20 and analysed with a Thermo Scientific Element 2 ICP-MS. The concentrations of sodium and potassium ($c_{element}$) were measured in each sample [mg/L]. The element content was then normalized to the weight of each sample dried at 105 °C ($m_{mortar,105^\circ C}$) and given [wt%/g mortar dried at 105 °C] as shown in Eq. (4):

$$Element \text{ content} = \frac{c_{element} \times V_{HNO_3}}{10^6 \times m_{mortar,105^\circ C}} \cdot 100\% \quad (4)$$

From the other twin test specimen, a small section of approx. 3 cm × 3 cm × 1 cm was cut out aligned to the exposed surface of each test specimen as shown in Fig. 3. The small blocks were epoxy impregnated, polished and carbon-coated for SEM-EDS analysis. The samples were analysed using a Hitachi S-3400 N scanning electron microscope (SEM) equipped with an energy dispersive spectrometer (EDS) from Oxford Instruments. SEM-EDS analyses of the matrix were performed with an acceleration voltage of 15 keV and a working distance of 10 mm. BSE images and elemental maps at a magnification of x1k were obtained along the exposed surfaces. Moreover, frames at x1.7k magnification were investigated with a minimum of 20 point-analyses of the matrix, representing the intermixed hydration phase assemblage at different depths below the exposed surface. The results of the point analyses were used for two different types of dot-plots. When the data of various elements are plotted over an independent element, in this case magnesium, the slopes of the resulting linear trend lines allow the determination of elemental ratios, e.g., Cl/Si, Na/Cl or K/Cl in a specific phase. The results were also plotted in graphs indicating the ideal compositions of various hydration phases, which allows the determination of the type of AFm phase intermixed in the matrix, or the Ca/Si ratio of the C-S-H [43]. It should be noted that the epoxy used for the preparation of the polished sections contained chlorine. Moreover, during sample preparation of the polished sections, ions from the pore solution can precipitate and might therefore be included in the EDS analysis of the cement paste. Both these effects should be kept in mind while interpreting the EDS results, even though we did not observe precipitated NaCl crystals in voids.

For the thermodynamic modelling of the changes in the phase assemblage upon exposure to the NaCl or the NaCl+KOH solution, we used the Gibbs free energy minimization software GEM-Selektor v.3 (GEMS3) [44–47]. The thermodynamic data from the PSI-GEMS database was expanded with a cement-specific database (CEMDATA 18) [48,49], which includes solubility products and solids relevant for cementitious materials. In addition, the CSHQ model proposed by Kulik was used to model the C-S-H phase in these systems [50].

The modelling approach used in this study is similar to the approaches described elsewhere [51,52]. We focused on the cement paste because we assume the sand in the mortar to be inert. Hydrated cement paste was modelled to be in equilibrium with increasing amounts of either the NaCl or the NaCl+KOH solution. We simulated the conditions in the mortar towards the exposed surface by increasing the amount of chloride solution with which the hydrated binder is in contact. However, in these models, transport is not taken into account, and thermodynamic equilibrium is assumed. This means that these models are neither time- nor space-resolved.

The cement paste consisted of 45 g of mixing water and 100 g of the CEM VI (S-V) composite cement, containing 47 wt% CEM I, 43 wt% GGBFS, and 10 wt% FA. The reaction degrees of the CEM I, the GGBFS, and the FA were assumed to be 90%, 60% and 20% respectively, representing 154 days of hydration. Unexposed cement paste and its components have been fully characterized in a hydration study reported by EnDurCrete [53,54].

The composition of the NaCl and NaCl+KOH exposure solutions were defined as described in the experimental programme as 30 g NaCl in 970 g H₂O and an additional 8.416 g KOH in the case of the NaCl+KOH solution.

The formation of the following phases was blocked in the software: gibbsite, kaolinite, graphite, dolomite, thaumasite, iron carbonates (incl. siderite), hematite, magnetite, goethite, pyrite, troilite, sulphur, and quartz. This was done in order to prevent the prediction of phases whose formation is thermodynamically possible, but kinetically impossible in the laboratory conditions applied in the experiments (temperature, pressure).

3. Results

3.1. Thermodynamic modelling

Fig. 4 shows the modelled phase assemblage of the hydrated CEM VI (S-V) binder upon exposure to a) the NaCl or b) the NaCl+KOH solution and the pH of the liquid phase. The experimental set-up is simulated by exposing a hydrated cement paste to increasing amounts of exposure solution.

Fig. 4 shows the mass of the predicted solid phases. The phase assemblage before exposure (no solution added) is the same for both simulations and consists of unreacted Portland cement, GGBFS, fly ash, and various hydration phases, such as C-S-H, CH, ettringite, monosulphate, hemicarbonate, hydrotalcite, and a siliceous hydrogarnet (Si-hydrogarnet). One can observe that the phases start to change when the binder is exposed to more than 0.01 L exposure solution per 100 g of binder, irrespective of which exposure solution. Upon exposure to larger amounts of the chloride solutions, Kuzel's salt and later Friedel's salt are predicted to form at the expense of monosulphate. This transformation in AFm phases is commonly observed upon chloride exposure [7]. It should be noted that, due to a lack of thermodynamic data, the chloride binding by hydrotalcite was not taken into account in the modelling, even though hydrotalcite is able to bind considerable amounts of chloride [21]. At high volumes of added NaCl solution, the formation of large quantities of M-S-H and zeolites was predicted by the model. However, these phases were not observed experimentally. This could be explained in two ways. On the one hand, the formation of specific phases can be kinetically hindered and they might therefore not be detected experimentally. On the other hand, the modelling routine applied here does not exactly represent the experimental conditions. In the laboratory, the exposure solutions were replaced weekly, which causes the removal of ions from the system whereas the modelling represents the equilibrium in a closed system.

In the case of NaCl exposure, the cement paste starts to dissolve considerably and lose mass from the point when the binder is exposed to more than 10 L solution per 100 g binder, whereas in the case of NaCl + KOH, the weight loss is more gradual and a large reduction in mass is only observed after 100 L of exposure solution. It can also be seen that less NaCl solution is required to dissolve and leach out portlandite (CH) and C-S-H than with the NaCl+KOH solution. So, the thermodynamic model confirms that the addition of KOH to the exposure solution (NaCl+KOH) reduces the leaching load compared to the pure NaCl solution. This can be explained by the difference in the pH between both predictions. Fig. 4 shows that the pH of the liquid phase first slightly

increases upon addition of both exposure solution. This slight increase in pH upon the addition of NaCl solution has been observed and explained previously in [15]. In the case of NaCl exposure, the pH starts to drop when the volume of the exposure solution surpasses approx. 0.1 L, and reaches down to approx. 11 at high volumes of NaCl exposure solution. In the case of NaCl+KOH exposure, the pH remains above 13 independent of the volume of exposure solution. It should be noted that the model predicts one liquid phase comprising both the pore solution and exposure solution in equilibrium with the phase assemblage of the hydrated cement paste. However, one cannot directly link the modelled pH of the liquid phase to the pH of the pore solution in the investigated mortar samples as the model does not account for transport nor for exchanging of the exposure solution.

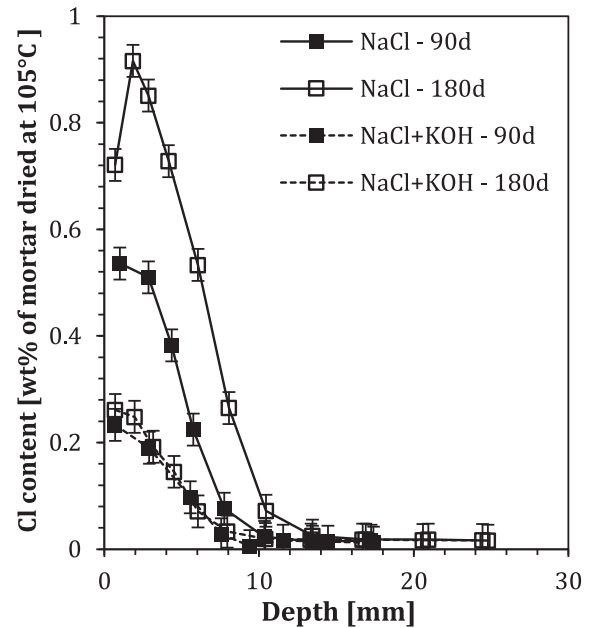


Fig. 5. Total chloride profiles for the mortar specimens exposed to NaCl or NaCl+KOH solution for 90 or 180 days, given as the total chloride content [wt % of mortar dried at 105 °C] as a function of depth below the exposed surface determined using potentiometric titration.

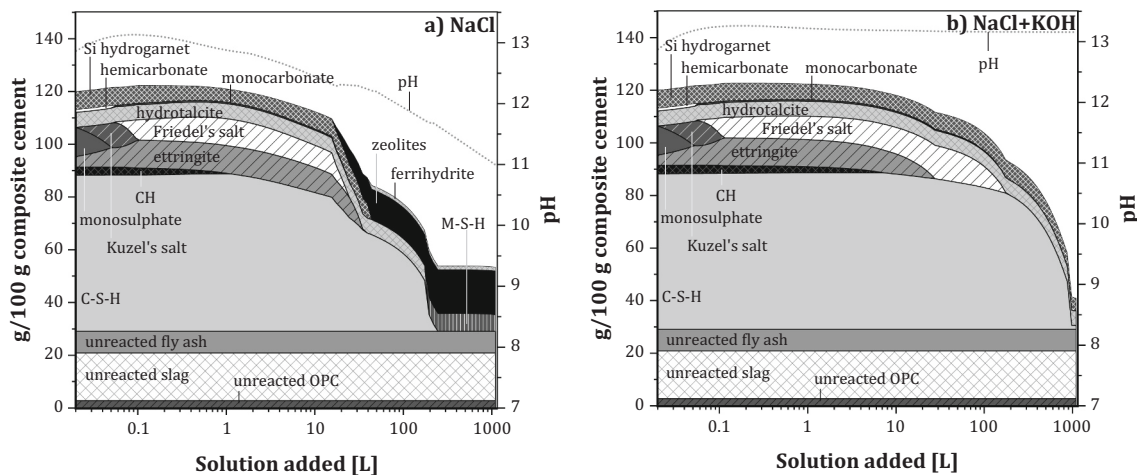


Fig. 4. Modelled phase assemblage [g/100 g composite cement] plotted as a function of added exposure solution [L] per 100 g of composite cement for the hydrated CEM VI (S-V) binder with a w/c ratio of 0.45 at 20 °C exposed to increasing amounts of a) the NaCl solution and b) the NaCl+KOH solution. In addition, the pH value of the liquid phase predicted by the modelling is indicated for both exposure scenarios.

3.2. Total chloride profiles

Fig. 5 shows the total chloride content of the mortar specimens exposed to the NaCl and the NaCl+KOH solution for 90 or 180 days as a function of depth below the exposed surface. Chlorides have penetrated into all the mortar specimens, but there are differences in the total chloride content and the chloride ingress depth with time.

The specimens exposed to the NaCl solution show about double or triple the maximum total chloride contents (0.5 wt% and 0.9 wt% after 90 and 180 days respectively) compared to the specimens exposed to the NaCl+KOH solution (0.3 wt% after both exposure times).

The total chloride content and the chloride ingress depth increased in the NaCl specimens over time from 90 to 180 days of exposure. After 180 days, the total chloride profile of the NaCl specimens shows typical peaking behaviour, in that the outermost section shows a lower total chloride content than the section slightly deeper in. This peaking shape is commonly observed in total chloride profiles after long-term exposure to chloride-containing solutions or sea water [6,30,55,56].

For the specimens exposed to the NaCl+KOH solution, the total chloride profile obtained after 90 days of exposure is very similar to the total chloride profile obtained after 180 days of exposure.

These results illustrate that the two different exposure solutions used in this study have very different impacts on the total chloride profiles obtained after 90 and 180 days of exposure.

3.3. TGA results

3.3.1. DTG curves

Fig. 6 shows the derivative thermogravimetric (DTG) curves in the temperature range of 250–500 °C obtained on powders from various depths below the exposed surface of the mortar specimens exposed to the NaCl solution (Fig. 6 a) and NaCl+KOH solution (Fig. 6 b) for 180 days. The temperature ranges for the decomposition of AFm phases and portlandite (CH) are indicated in Fig. 6.

In both specimens, the portlandite content decreases towards the

exposed surface. In the NaCl exposed specimen, the portlandite peak even disappears in the outermost section.

The weight loss peaks in the AFm region seem to increase towards the exposed surface for both specimens. Note that, with decreasing depth below the exposed surface, the peak in the temperature range of AFm decomposition shifts towards lower temperatures and shows a double peak for both exposures. The single peak in the unaffected sections (e.g. 25 mm) has been associated with hydrotalcite or carbonate AFm [21,41]. The double peak has been related to the decomposition of chloride-containing AFm phases [13,21,32].

3.3.2. Portlandite profiles and AFm weight loss profiles

Fig. 7 shows the portlandite content determined by TGA in the mortar specimens exposed to the NaCl and NaCl+KOH solutions as a function of depth below the exposed surface after 90 days and 180 days of exposure.

The portlandite content decreases towards the exposed surface in all specimens. This is expected as calcium ions are leached from the surface of the specimens immersed in solutions that are not saturated with respect to calcium, leading to the dissolution of portlandite. The specimens exposed to the NaCl solution no longer contain portlandite in the outermost sections, while the NaCl+KOH specimens still contain a certain amount of portlandite in all sections.

With exposure time, the portlandite content in the specimens exposed to the NaCl solution continues to decrease in the sections down to a depth of 12 mm. This trend is not observed for the NaCl+KOH specimens, which show similar portlandite profiles after 90 and 180 days of exposure. The leaching of portlandite is considerably slower with exposure to NaCl+KOH than to NaCl, showing as intended that the set-up chosen in this study can limit the leaching of calcium.

The difference in solubility of the portlandite for the two exposure solutions can also be demonstrated with thermodynamic modelling. We calculated the calcium concentration for a simplified portlandite saturated system in equilibrium with the NaCl and NaCl+KOH solutions. The NaCl system resulted in a calcium concentration of about 0.034 mol/L

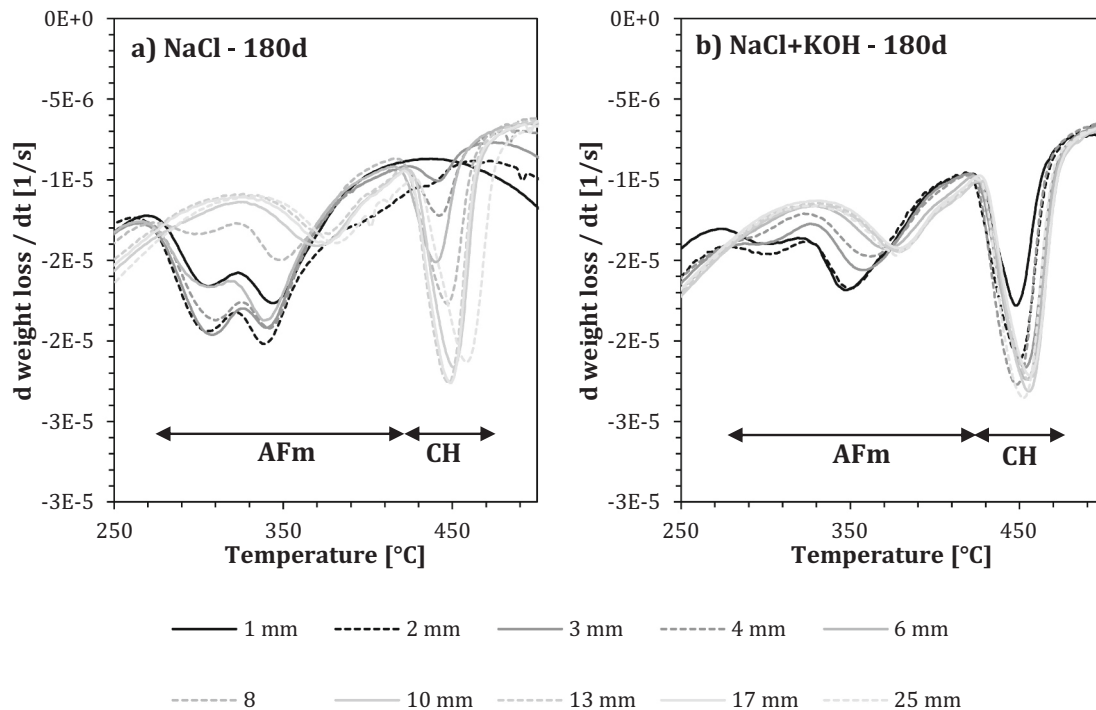


Fig. 6. DTG curves of sections at various depths below the exposed surface for specimens exposed a) to the NaCl solution and b) the NaCl+KOH solution for 180 days in the temperature range of AFm and portlandite (CH) decomposition (250–500 °C).

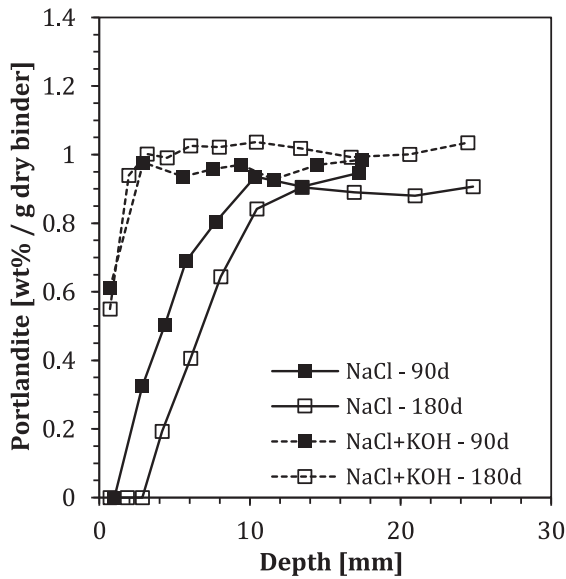


Fig. 7. Portlandite profiles for the mortar specimens exposed to the NaCl or the NaCl+KOH solution for 90 or 180 days, given as the portlandite content [wt%/g of dry mortar] determined with TGA as a function of depth below the exposed surface.

and a pH of 12.8, whereas the NaCl+KOH system had a calcium concentration of 0.007 mol/L at a pH of 13.2. The reduction in dissolution of portlandite ($\text{Ca}(\text{OH})_2 (s) \rightarrow \text{Ca}^{2+} + 2 \text{OH}^-$) upon increased hydroxyl concentration in the KOH system can be ascribed to the common ion effect.

Fig. 8 shows the profiles of the weight loss in the temperature interval related to AFm decomposition as a function of depth below the exposed surface. The background weight loss in this region is about 0.10 wt%. The weight loss relative to the background level increases between a depth of 10 mm and the exposed surface for the NaCl exposed specimen, whereas for the NaCl+KOH exposed specimen the weight loss only starts to increase from a depth of 5 mm below the exposed surface. There is also a considerable difference in the maximum level of the weight loss depending on the exposure solution. In the specimen exposed to the

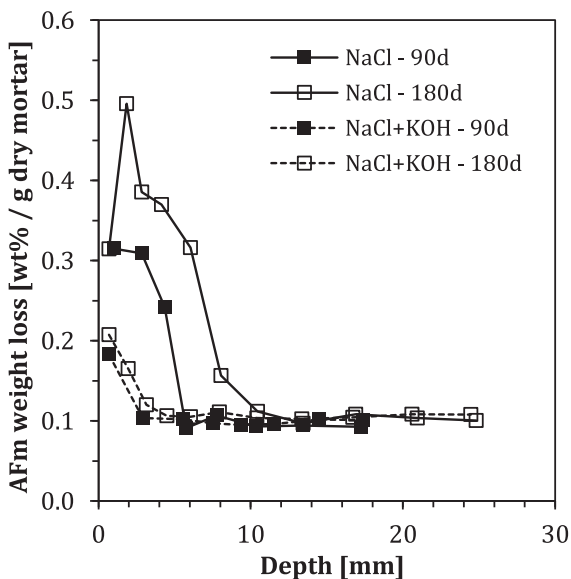


Fig. 8. Weight loss related to AFm profiles for the mortar specimens exposed to the NaCl or the NaCl+KOH solution for 90 or 180 days, given as [wt%/g of dry mortar] determined with TGA as a function of depth below the exposed surface.

NaCl solution, the maximum weight loss is as much as 0.50 wt% whereas the maximum for the specimen exposed to the NaCl+KOH solution is less than half, i.e., 0.20 wt%. Hemstad et al. [13] reported a similar increase in AFm weight loss upon moderate leaching of well-hydrated paste samples exposed to chlorides. However, such an increase is not predicted by the thermodynamic model in this study (see Fig. 4). It is possible that the aluminium needed for the formation of additional AFm phases could be liberated from the C-A-S-H upon moderate leaching, as reported by Baba Ahmadi et al. for calcium-deficient systems [57]. Further investigation will be required to elucidate what is causing the increase in chloride-containing AFm phases upon leaching.

It should be noted that the weight loss determined can only be used as a semi-quantitative indication, because the total specimen mass in the outermost sections could decrease due to leaching, which can lead to a relative enrichment of remaining phases, as mentioned in Section 2.3. Hence, a decrease in weight loss of a specific phase is not an artefact of leaching. On the contrary, leaching would lead to an underestimation of the decrease. For example, the decrease observed in the outermost section of the specimen exposed to the NaCl solution for 180 days compared to the adjacent section deeper in does reflect a real relative decrease in the weight loss related to AFm.

3.4. Sodium and potassium profiles

Fig. 9 shows the content of sodium (Na) and potassium (K) in the various sections of the mortar specimens exposed to the NaCl or NaCl+KOH solution for 90 and 180 days as a function of depth below the exposed surface.

Both specimens show an ingress of sodium from the exposed surface, i.e., from the exposure solution, into the specimen. The ingress observed is higher in the case of the exposure to NaCl+KOH than it is for NaCl.

The potassium concentration used in the NaCl+KOH exposure solution (150 mmol/L) was based on a rough estimate of the potassium concentration in the pore solution of the mortar. However, the potassium content in both the NaCl+KOH and the NaCl exposed specimens decreases towards the exposed surface. This indicates leaching of potassium from both specimens into the exposure solution. The potassium concentration in the pore solution of the mortar was underestimated in the preliminary calculations and must be higher than 150 mmol/L. The specimen exposed to the NaCl solution shows a slightly higher degree of potassium leaching than the specimen exposed to the NaCl+KOH solution, as can be expected.

It should be noted that the sodium and potassium profiles did not change significantly between 90 and 180 days. No further ingress of sodium or leaching of potassium was observed after 90 days of exposure.

3.5. Microstructure and elemental maps after exposure

Fig. 10 shows the BSE images, and silicon (Si), sodium (Na), potassium (K), chlorine (Cl) and calcium (Ca) maps of the two mortar specimens after exposure to a) the NaCl solution and b) the NaCl+KOH solution for 180 days. The top side of the image represents the exposed surface.

In both samples, the porosity increases and the calcium content decreases towards the exposed surface. There seems to be a clear increase in porosity and a decrease in silicon towards the exposed surface only with exposure to NaCl+KOH. The specimen exposed to the NaCl solution shows a slight increase in porosity and no decrease in silicon towards the exposed surface. This difference can be explained by the fact that the solubility of silicon increases exponentially with increasing pH above pH 8 [58], which affects the solubility of C-S-H at high pH [59,60]. The considerably higher pH of the NaCl+KOH solution (approx. pH 13.2, according to GEMS calculations) seems therefore to have caused leaching of silicon from the outermost sections of the specimen into the NaCl+KOH exposure solution. C-S-H represents the largest fraction of hydration phases in the cement paste matrix, so leaching of this phase

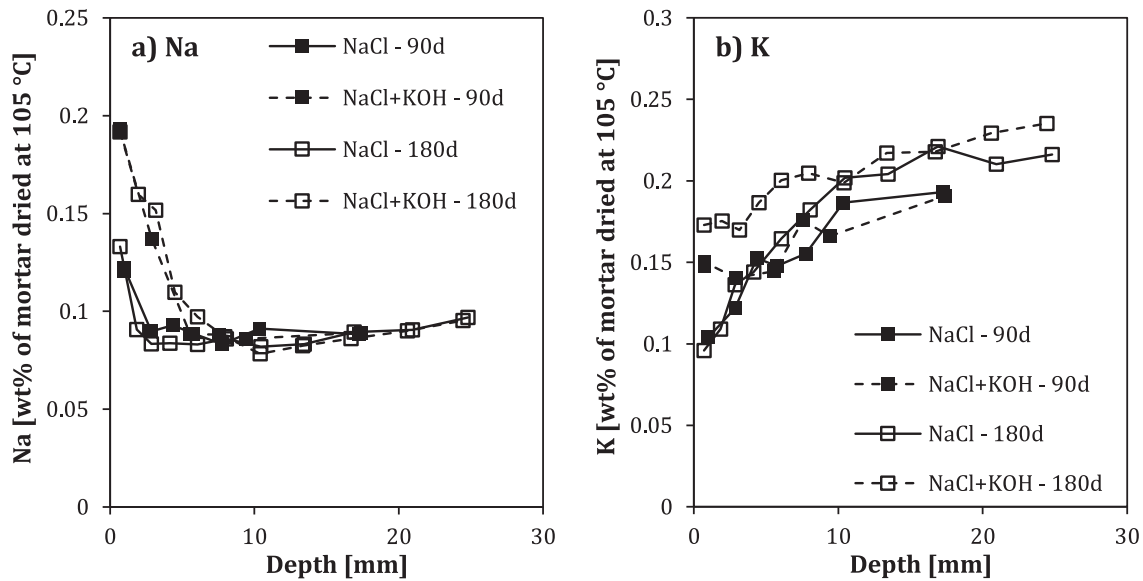


Fig. 9. Elemental profiles of a) sodium (Na), b) potassium (K), for the mortar specimens exposed to the NaCl solution (solid lines) and the NaCl+KOH solution (dashed lines) for 90 days (filled squares) or 180 days (hollow squares) given as element content [wt% of mortar dried at 105 °C] as a function of depth below the exposed surface determined with ICP-MS.

results in a significant increase in porosity. However, this leaching of C-S-H is limited to the outermost 200 μm of the specimen exposed to NaCl+KOH.

The SEM-EDS maps are only semi-quantitative, so this overall decrease in specimen mass also leads to a reduction in signal in all other elemental maps. For the calcium content in particular, this might at first sight seem to contradict the portlandite profiles, which show a higher portlandite and thereby also calcium content in the NaCl+KOH specimens than in the NaCl specimens (see Fig. 7). However, the portlandite profiles cannot be directly compared to the SEM-EDS maps (Fig. 10), because the latter only represent the outermost 1–2 mm of the specimen, while the portlandite profiles (Fig. 7) are obtained down to a depth of 25 mm, where each data point represents the average CH content in each section.

Moreover, the precipitation of a calcium-rich layer on top of the exposed surface in the specimen exposed to the NaCl solution can be observed in Fig. 10. This layer is assumed to be a calcite layer because no portlandite was detected by TGA in the outermost section (see Fig. 7). The specimens were stored in $\text{Ca}(\text{OH})_2$ saturated water prior to exposure, so a portlandite layer probably formed during exposure and later carbonated to CaCO_3 during sample preparation. This layer can be observed in the case of exposure to the NaCl solution, but not in the case of exposure to NaCl+KOH. A simple thermodynamic calculation of a CaCO_3 saturated system in equilibrium with each of the solutions shows that the calcium concentration in the case of NaCl exposure is 0.65 mmol/L at a pH of approx. 10 compared to a calcium concentration of 0.70 mmol/L at a pH of 13.1 for the NaCl+KOH exposure. This indicates that the degree of undersaturation of carbonates increases slightly with increasing pH, which means that, in the case of exposure to the NaCl+KOH solution, the carbonate layer might have dissolved more than it would with NaCl exposure. However, it should be noted that there is still a trace of calcite visible on the NaCl+KOH exposed mortar, which could indicate that the calcite surface layer has just fallen off in the case of the NaCl+KOH exposed mortar because the surface has disintegrated more than the NaCl exposed mortar.

The chlorine maps in Fig. 10 show a higher maximum chlorine content in the specimen exposed to the NaCl solution than in the specimen exposed to the NaCl+KOH solution. Moreover, the chlorine content measured with EDS is observed to decrease slightly towards the exposed surface, similar to the calcium content in both specimens.

The SEM-EDS maps shown in Fig. 10 also enable us to comment on the impact of the preparation of the polished sections on the EDS results. As mentioned in the methods section, the epoxy used for the impregnation contains chlorides. This can be seen in Fig. 10 in the slightly higher chloride intensities above the exposed surface, which consists only of epoxy. A decrease in the intensity of the chloride maps can be seen in the outermost 200 μm of the mortar followed by an increase in the intensity slightly deeper in. These observations correlate with the results of the total chloride profiles and demonstrate that we can use the EDS analysis to describe relative differences in the chloride content of the paste.

3.6. Changes in the C-S-H and AFm composition due to chloride exposure

In the cement paste, chlorides are bound either chemically in AFm phases, such as Friedel's salt or Kuzel's salt, or physically by their accumulation in the diffusive layer of the C-S-H. We therefore investigated in detail the changes in C-S-H and AFm composition as a function of depth below the exposed surface, with SEM-EDS point analyses at various depths below the exposed surface in specimens after 180 days of exposure.

3.6.1. Changes in the C-S-H composition

Fig. 11 shows the Cl/Mg over the Si/Mg ratio of the EDS point analyses performed on the matrix of the mortar specimens exposed to a) the NaCl solution and b) the NaCl+KOH solution for 180 days. The results shown in Fig. 11 were taken at depths of 0.03–20 mm below the exposed surfaces, as indicated by the different heat map colours. The coloured trend lines indicate the Cl/Si ratio determined for the results of each analysed depth, corresponding to the Cl/Si ratio of the C-S-H phase at that depth.

The Cl/Si ratio of the C-S-H in the specimen exposed to the NaCl solution is lower at depths of 0.03 mm and 0.3 mm than it is deeper into the specimen (at depths of 0.6–4 mm). From 4 mm onwards, the Cl/Si ratio decreases again with increasing depth below the exposed surface.

In the case of the specimen exposed to the NaCl+KOH solution, the highest Cl/Si ratio was determined in the outermost section at a depth of 0.03 mm. For all depths investigated, the Cl/Si ratio decreased with increasing depth below the exposed surface from 0.03–4 mm and seems to reach a constant value from 10 mm onwards, reflecting the Cl/Si

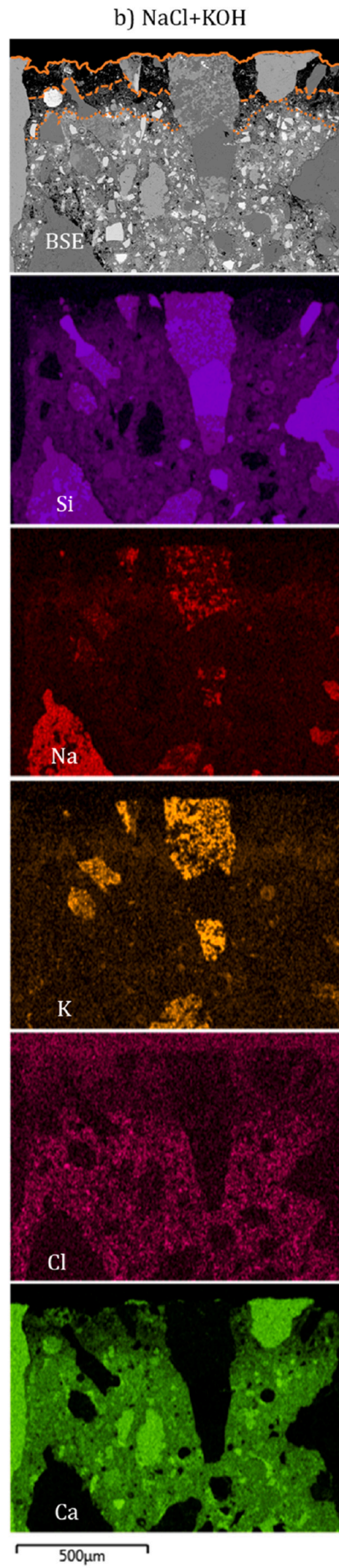
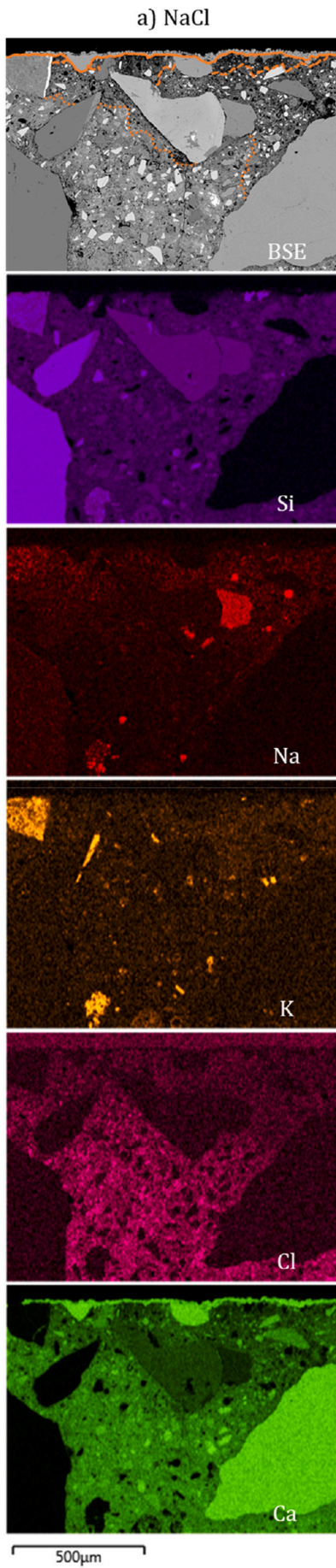


Fig. 10. BSE images, and silicon (Si), sodium (Na), potassium (K), chlorine (Cl) and calcium (Ca) maps of the mortar specimens exposed to a) the NaCl solution or b) the NaCl+KOH solution for 180 days. The exposed surface is located at the top of each image, indicated with a solid line in the BSE image. Dashed and dotted lines indicate differently leached zones in both BSE images.

background level of the specimen.

The background level of the Cl/Si ratio is independent of the exposure solution and is about 0.02 for both specimens. Theoretically, one might expect the background level of the Cl/Si ratio to approach zero. However, low chloride background levels can originate from the cement and from the epoxy used to impregnate the SEM-EDS sample. This chloride background level is then enlarged as we divide it by the low magnesium levels in the volume analysed by EDS. The overall trends observed, however, are not affected by this.

If we compare the maximum Cl/Si ratios obtained, the specimen exposed to the NaCl solution shows a considerably higher maximum Cl/Si ratio (about 0.2) than the specimen exposed to the NaCl+KOH solution (about 0.07), with the exception of the results at a depth of 0.03 mm in the NaCl+KOH specimen.

To investigate the changes in the C-S-H composition that can lead to the changes in its Cl/Si ratio, we investigated the Si/Ca ratio of the C-S-H at depths from 0.03–20 mm below the exposed surface. Fig. 12 shows the results of the Al/Ca over the Si/Ca ratio of the EDS point analyses performed on the matrix of the mortar specimens exposed to a) the NaCl solution, and b) the NaCl+KOH solution for 180 days. This way of plotting allows the determination of the Si/Ca ratio of the C-S-H by framing the data clouds between lines reaching to the AFm and CH ideal compositions [43].

Fig. 12 shows that the Si/Ca ratio does not change much between depths of 0.3 mm and 20 mm in either exposure solution. At depths of 0.3 mm and greater, the Si/Ca ratio determined is the same in both specimens. Changes in the Si/Ca ratio of the C-S-H are only observed between depths of 0.03 and 0.3 mm.

The results obtained at a depth of 0.03 mm in the specimen exposed

to NaCl+KOH are not assumed to be C-S-H. The results show a very high scatter and mostly plot close to the ideal composition of portlandite (CH), which does not contain any silicon. This can be explained by the leaching of silicon from the outermost sections of the specimen exposed to the NaCl+KOH solution due to the high pH of this exposure solution, as described in 3.5. Taking this information into account, the Cl/Si ratio (see Fig. 11 b) determined for the C-S-H at this depth in the specimen exposed to the NaCl+KOH solution should be considered as an artefact, because the significantly lower silicon content in this data had the consequence of artificially increasing the Cl/Si ratio. The results obtained in the specimen exposed to the NaCl solution and the results from deeper sections of the specimen exposed to the NaCl+KOH solution, however, represent commonly observed C-S-H data clouds.

While the results shown in Fig. 12 indicate no change in the Si/Ca ratio of the C-S-H below a depth of 0.3 mm, the question arises of how the Si/Ca ratio of the C-S-H phases is affected by the chloride exposure and the type of chloride solution in the outermost sections (0.03–0.3 mm). Fig. 13 therefore shows the results obtained on the Al/Ca and the Si/Ca ratio of the C-S-H at depths of 0.03–0.3 mm.

For the specimen exposed to the NaCl solution, a clear trend is visible from a decalcified C-S-H (high Si/Ca ratio) to a sound C-S-H (medium Si/Ca ratio) with increasing depth below the exposed surface. In the case of the specimen exposed to the NaCl+KOH solution, there is no clear trend. The results obtained in the outermost section (0.03 mm) plot close to a silicon-free composition (e.g., CH) and not to a decalcified C-S-H composition. With increasing depth below the exposed surface, the same Si/Ca ratio as in the specimen exposed to the NaCl solution was measured.

Fig. 14 shows the Na/Mg over the Si/Mg ratio of the EDS point

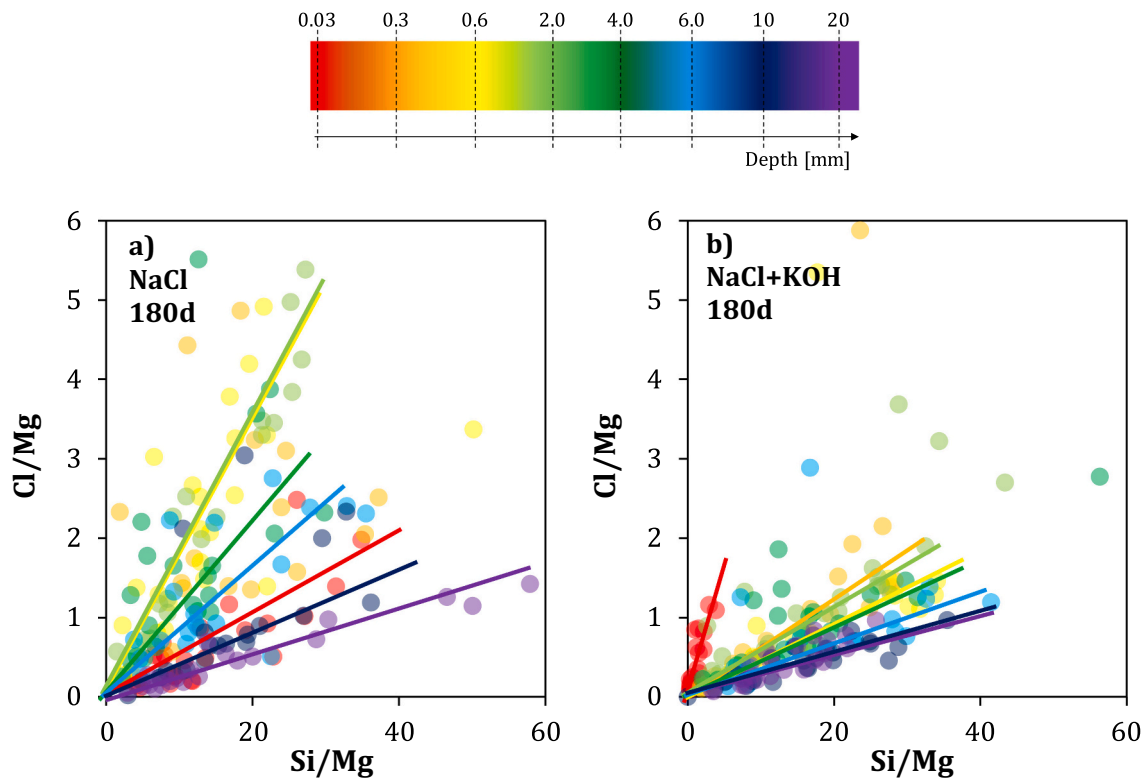


Fig. 11. Cl/Mg ratio over the Si/Mg ratio for the point analyses of the matrix at depths of 0.03–20 mm below the exposed surface. The lines indicate the Cl/Si ratio of the C-S-H phase at the various depths.

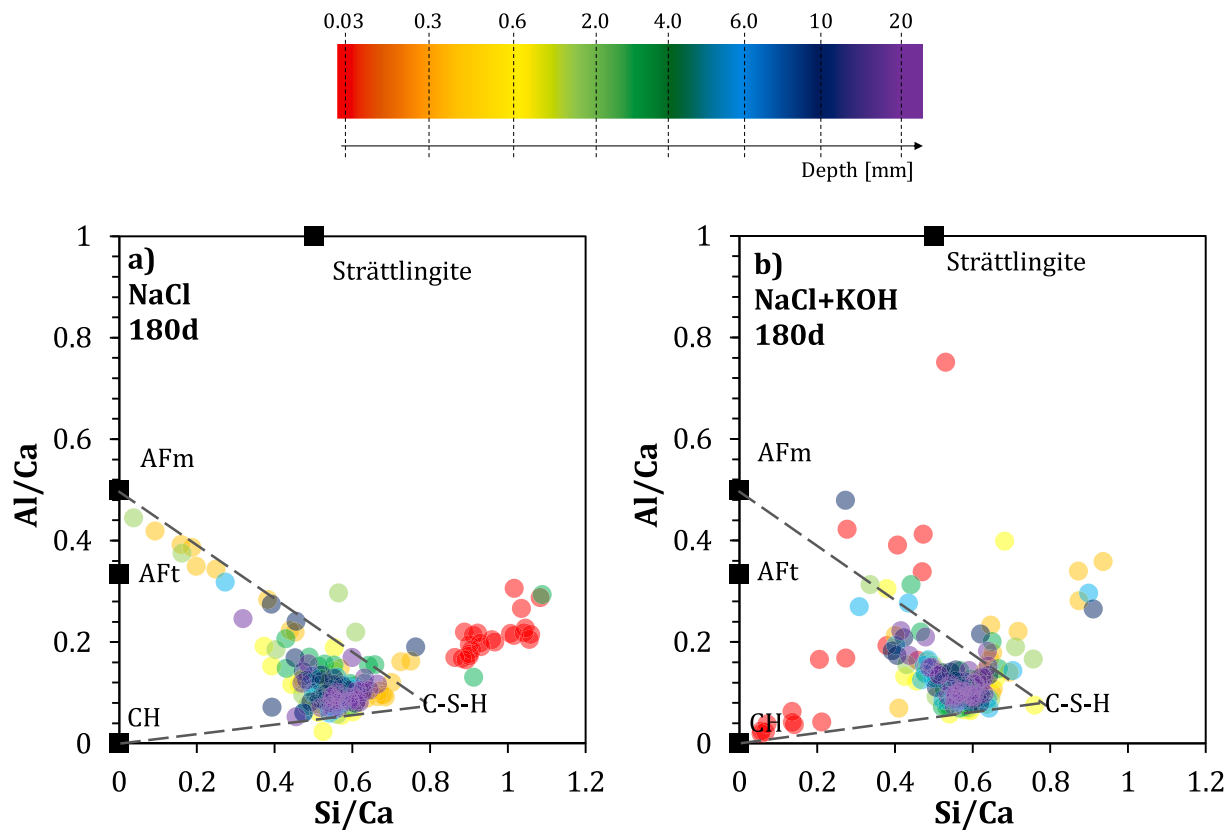


Fig. 12. Al/Ca ratio over the Si/Ca ratio for the point analyses of the matrix at depths of 0.03–20 mm below the exposed surface. The ideal compositions of portlandite (CH), ettringite (AFt) and AFm phases are indicated. The composition of the C-S-H is estimated by framing it with tangents (dashed lines) reaching to the AFm and CH compositions.

analyses performed on the matrix of the mortar specimens exposed to a) the NaCl solution, and b) the NaCl+KOH solution for 180 days. The coloured lines in Fig. 14 indicate the Na/Si ratio of the C-S-H phase at the various depths below the exposed surface.

In the specimen exposed to the NaCl solution, the outermost section (0.03 mm) shows a high Na/Si ratio of approx. 0.1. With increasing depth from 0.03 mm to 2.0 mm, the Na/Si ratio in the specimen decreases. At depths greater than 2.0 mm, the Na/Si ratio seems to oscillate around the background level of approx. 0.02, and these variations are assumed to be within the margin of error.

In the specimen exposed to the NaCl+KOH solution, the Na/Si ratio of the C-S-H also decreases with increasing depth below the exposed surface. The only exception to this is the Na/Si ratio obtained at 0.6 mm, which is lower than the Na/Si ratio obtained at a depth of 2.0 mm. Note that the data points obtained at a depth of 0.03 mm do not represent C-S-H due to leaching of silicon in the outermost sections. The Na/Si ratios obtained at depths between 6.0 mm and 20 mm oscillate around the same background level as for the specimen exposed to the NaCl solution, approx. 0.02. These depths are therefore assumed to represent the background Na/Si ratio of the unaffected matrix samples.

The relatively high Na/Si ratios determined for both specimens in the range between 0.6 mm and 4.0 mm were not expected, because sound (not de-calcified) C-S-H is reported to adsorb only minor amounts of alkalis [30,61], and the Ca/Si ratio of the C-S-H was found to be unaffected at depths greater than 0.3 mm. The higher Na content in the outer sections might therefore be due to a higher Na concentration in the pore solution.

Fig. 15 shows the K/Mg over the Si/Mg ratio of the EDS point analyses performed on the matrix of the mortar specimens exposed to a) the NaCl solution, and b) the NaCl+KOH solution for 180 days. The coloured lines in Fig. 15 indicate the K/Si ratio of the C-S-H phase at the

various depths below the exposed surface.

The highest K/Si ratio can be found in both specimens at the relatively greater depths of approx. 10 to 20 mm. This K/Si ratio describes the level of potassium in the unaffected matrix samples and is therefore the same in both specimens (approx. 0.04). The K/Si ratio then decreases from the background level towards the exposed surface for both specimens. However, it should be noted that the outermost section (at a depth of 0.03 mm) in the specimen exposed to the NaCl solution showed a considerably higher K/Si ratio (approx. 0.02) than sections even slightly below it (approx. 0.01).

As described for the Na/Si ratio, the high K/Si ratio determined for the outermost section in the specimen exposed to the NaCl+KOH solution is most likely an artefact of the low silicon content measured in this section and does not represent C-S-H.

The lowest K/Si ratios are observed for the specimen exposed to the NaCl solution at depths of 0.3 to 4.0 mm (approx. 0.01). The specimen exposed to the NaCl+KOH solution showed higher K/Si ratios (approx. 0.02–0.04) at these depths (0.6 to 4.0 mm). This indicates a lower degree of potassium leaching in the case of exposure to the NaCl+KOH solution than with the NaCl solution, which is expected and agrees with the ICP-MS results (see Fig. 9 b)).

3.6.2. Changes in the AFm composition

To determine the type of AFm phases present in the specimens at the various depths below the exposed surface, different ways of plotting are needed. As a first step, the results at depths from 0.03–20 mm are plotted as the S/Ca over the Al/Ca ratio in Fig. 16 a) for the specimen exposed to the NaCl solution and in Fig. 16 b) for the specimen exposed to the NaCl+KOH solution.

The data points obtained at a depth of 0.03 mm in the specimen exposed to the NaCl solution only plot in the proximity of the x-axis

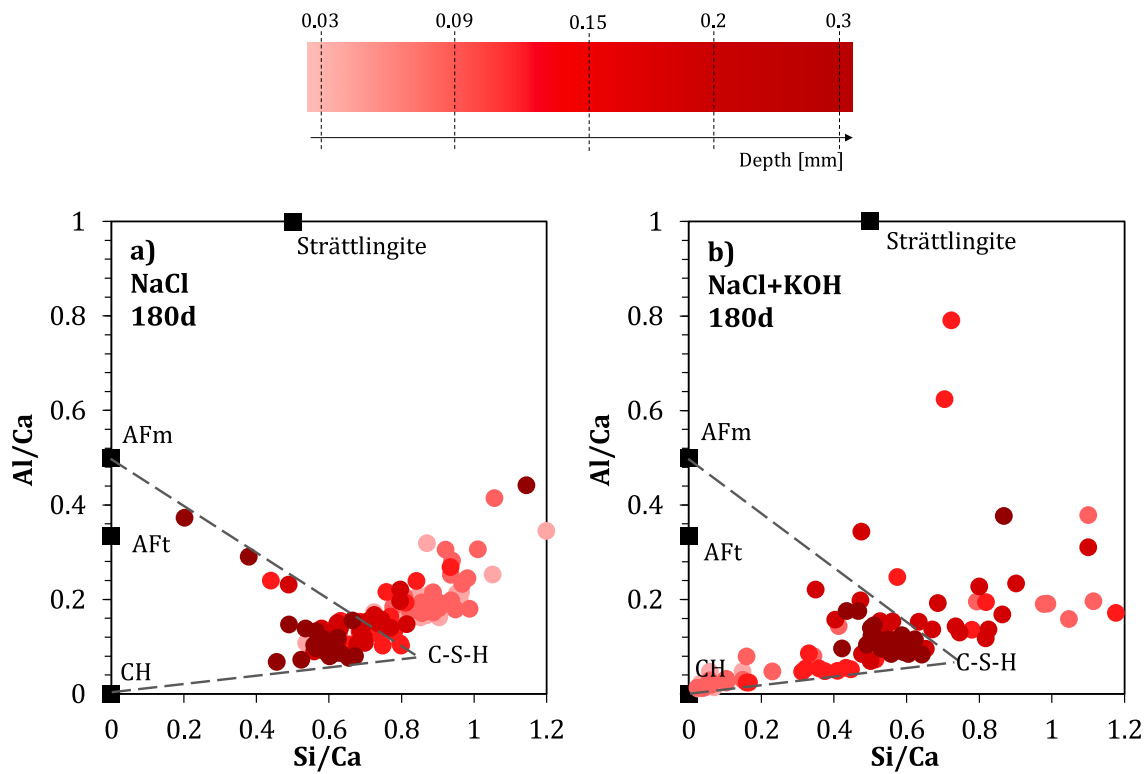


Fig. 13. Al/Ca ratio over the Si/Ca ratio for the point analyses of the matrix at depths of 0.03–0.3 mm below the exposed surface. The ideal compositions of portlandite (CH), ettringite (AFt) and AFm phases are indicated. The composition of the C-S-H is estimated by framing it with tangents (dashed lines) reaching to the AFm and CH compositions. The tangents shown are fitted to the datapoint at 0.3 mm depth as a guide for the eye.

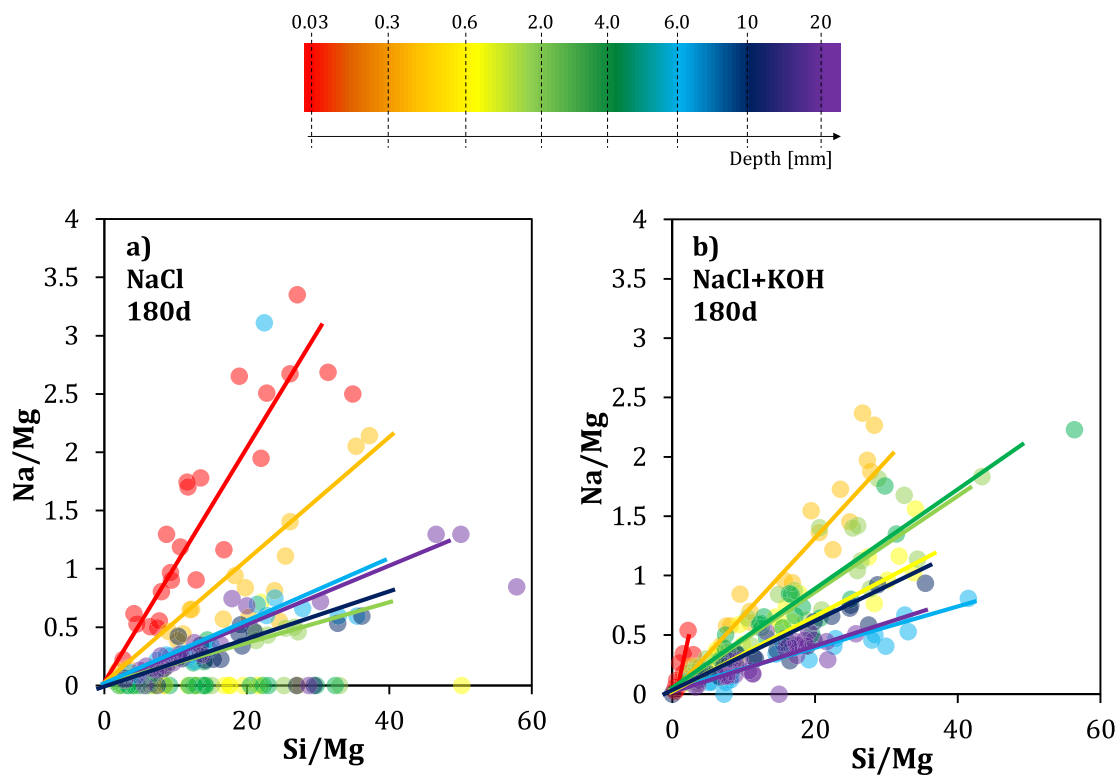


Fig. 14. Na/Mg ratio over the Si/Mg ratio for the point analyses of the matrix at depths of 0.03–20 mm below the exposed surface. The lines indicate the Na/Si ratio of the C-S-H phase at the various depths.

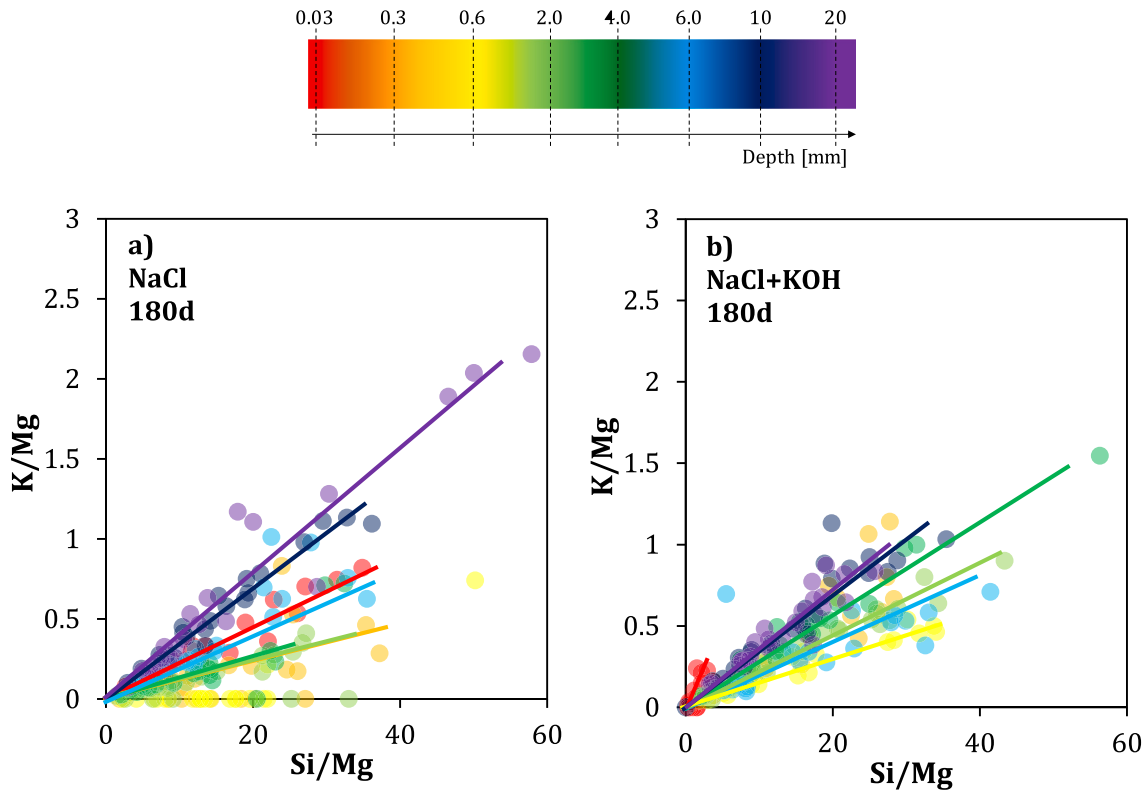


Fig. 15. K/Mg ratio over the Si/Mg ratio for the point analyses of the matrix at depths of 0.03–20 mm below the exposed surface. The lines indicate the K/Si ratio of the C-S-H phase at the various depths.

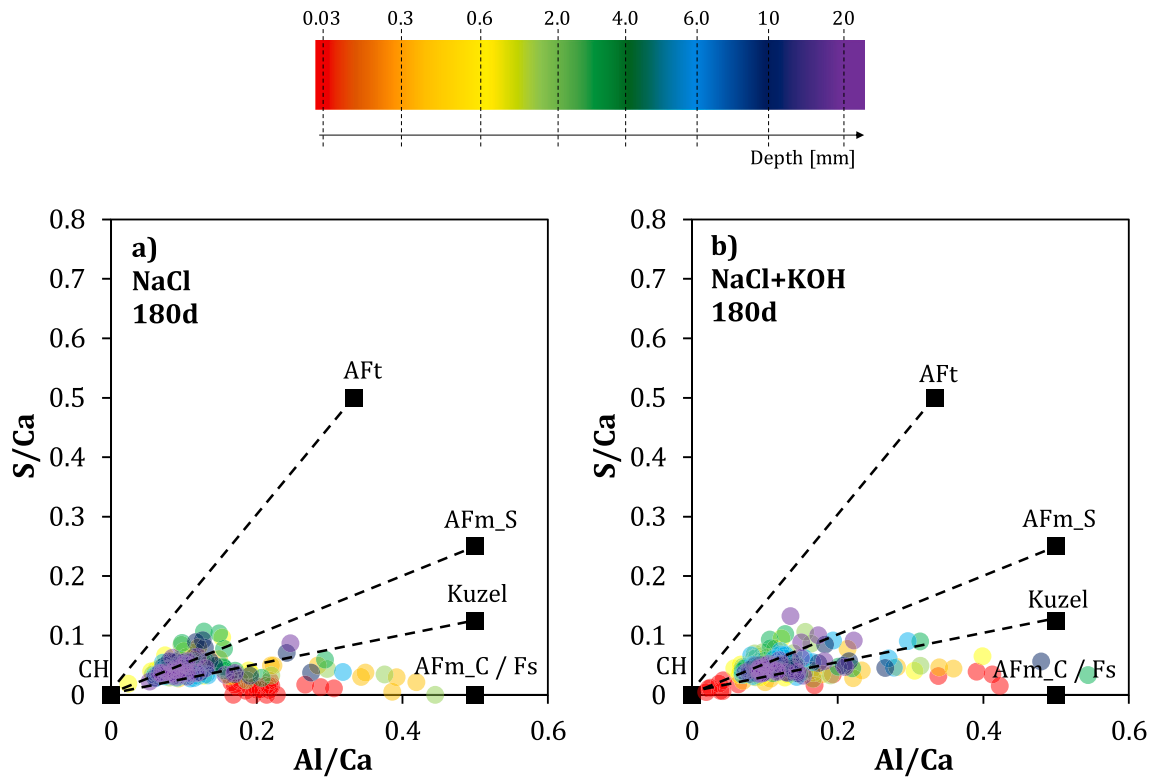


Fig. 16. S/Ca ratio over the Al/Ca ratio for the point analyses of the matrix at depths of 0.03–20 mm below the exposed surface. The ideal compositions of portlandite (CH), ettringite (AFt), monosulphate (AFm_S), Kuzel's salt (Kuzel), monocarbonate (AFm_C) and Friedel's salt (Fs) are indicated.

pointing towards the monocarbonate (*AFm_C*) or Friedel's salt (*Fs*) composition. With increasing depth below the exposed surface, some of the data points obtained from the specimen exposed to the NaCl solution still point towards the composition of monocarbonate or Friedel's salt, while others plot a line pointing towards the composition of monosulphate (*AFm_S*). The presence of monosulphate is in agreement with the GEMS modelling results of the hydrate phase assemblage in the unaffected matrix samples (see Fig. 4). Moreover, ettringite and small amounts of hemicarbonate are predicted to form in the GEMS model upon hydration of the cement, due to traces of limestone in the binder (approx. 0.1 wt%). These phases were also detected experimentally on unexposed hydrated paste samples [53] (results not shown here), but were not detected experimentally by SEM-EDS. This is probably due to the small amounts of hemicarbonate present and the difficulty of detecting ettringite with EDS [22].

The results obtained on the specimen exposed to the NaCl+KOH solution show similar results to those for the specimen exposed to the NaCl solution. The difference between the two specimens is only visible in the results obtained at a depth of 0.03 mm in Fig. 16. Some of the data points obtained in the outermost section (0.03 mm) in the specimen exposed to NaCl+KOH, as with all other data points, plot on a line pointing towards the composition of monosulphate, while others plot a line towards the composition of monocarbonate or Friedel's salt.

As Friedel's salt and monocarbonate cannot be distinguished in Fig. 16, the same data points are replotted in Fig. 17, but now showing the Cl/Ca over the Al/Ca ratio. This way of plotting can distinguish the AFm phases by their chloride content.

For the specimen exposed to the NaCl solution, the results with the highest Cl/Ca ratios were obtained at depths of 0.6–4 mm. This agrees with the results of the total chloride profiles (see Fig. 5) since the highest total chloride content was measured at these depths below the exposed surface. The data points from 0.6–4 mm plot on a line pointing towards

the composition of Friedel's salt. Both at higher and lower depths, the Cl/Ca ratios are lower than those obtained between 0.6 and 4 mm, indicating the presence of AFm phases containing less chloride than Friedel's salt (Kuzel's salt) or no chloride (e.g., monosulphate).

In the case of the specimen exposed to the NaCl+KOH solution, the results with the highest Cl/Ca ratios were obtained in the outermost section (0.03 mm). This agrees well with the results of total chloride profiles (see Fig. 5). The data points at a depth of 0.03 mm plot on a line pointing towards the composition of Kuzel's salt. As Kuzel's salt contains less chloride per mol than Friedel's salt, this indicates a lower chemically bound chloride content in the specimen exposed to the NaCl+KOH solution than in the specimen exposed to the NaCl solution. With increasing depth below the exposed surface, the Cl/Ca ratio decreases, reaching similar background values to those obtained in the specimen exposed to the NaCl solution.

At depths of 10 mm and below, the data points plot mostly along the horizontal axis in Fig. 17, indicating the presence of monosulphate or monocarbonate containing very little chloride. This is in agreement with the total chloride profiles, which do not show chloride ingress beyond 10 mm (Fig. 5).

4. Discussion

4.1. Impact of leaching on the total chloride content

To understand why the specimens exposed to the NaCl solution and the specimens exposed to NaCl+KOH solution have different total chloride profiles, we need to understand the effect of the two exposure solutions on the hydration phase assemblage and the microstructure of the mortars.

Fig. 18 shows the total chloride, portlandite, sodium and potassium profiles and the EDS elemental ratios determined for C-S-H (Cl/Si, Ca/

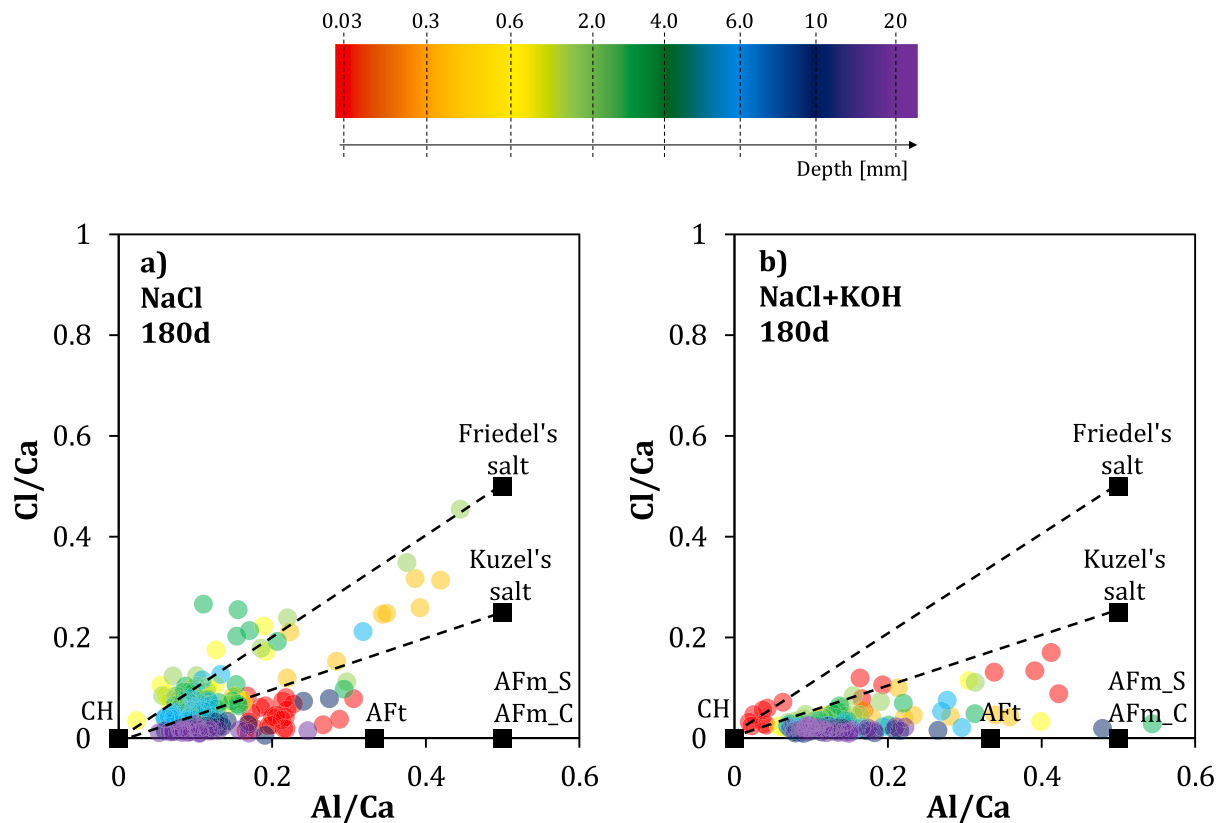


Fig. 17. Cl/Ca ratio over the Al/Ca ratio for the point analyses of the matrix at depths of 0.03–20 mm below the exposed surface. Black squares indicate the ideal compositions of portlandite (CH), Friedel's salt, Kuzel's salt, monosulphate (AFm_S), monocarbonate (AFm_C), and ettringite (AFt).

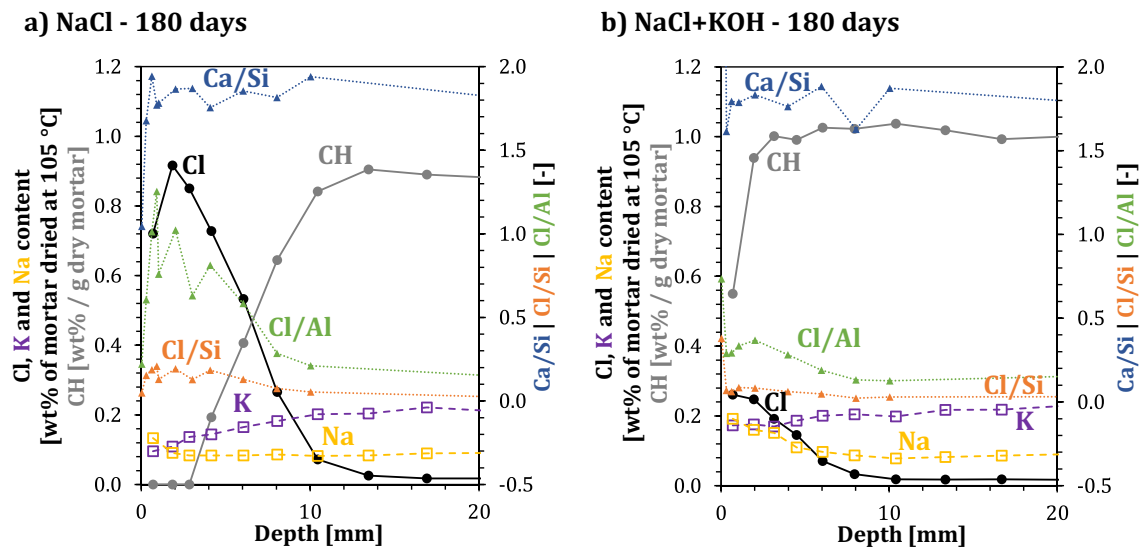


Fig. 18. Comparison of total chloride profiles (Cl, black circles) and portlandite profiles (CH, grey circles) with the potassium profiles (K, purple squares), sodium profiles (Na, yellow squares), Ca/Si ratios (blue triangles), Cl/Si ratios (orange triangles), and Cl/Al ratios (green triangles) of the matrix determined with SEM-EDS as a function of depth below the exposed surfaces of the mortar specimens exposed to a) the NaCl solution or b) the NaCl+KOH solution for 180 days. (For interpretation of the references to colour in this figure legend, the reader is referred to the web version of this article.)

Si) and AFm (Cl/Al) after 180 days of exposure as a function of depth for the two exposure solutions.

The portlandite and potassium profiles measured (see Figs. 7 and 9b) were used as indicators for the degree of leaching at the various depths below the exposed surface. Fig. 18 shows that the two leaching parameters are inversely correlated with the total chloride content in the mortar specimens. This inverse correlation is clearer for the mortar specimen exposed to NaCl solution than for the specimen exposed to the NaCl+KOH solution. The highest total chloride content is measured near the exposed surface where all the portlandite has leached out and where the potassium content is relatively low. Deeper below the exposed surface of the mortar specimen, the total chloride content decreases gradually, whereas the portlandite and potassium contents increase towards their background levels. The specimen that was exposed to the NaCl+KOH solution shows significantly less leaching of portlandite and potassium and a lower total chloride content than the specimen that was exposed to the NaCl solution.

The experimental set-up using the two exposure solutions NaCl and NaCl+KOH succeeded in provoking different levels of leaching and a considerable difference in the total chloride ingress profiles.

4.1.1. Increased porosity due to leaching

Leaching causes the dissolution of portlandite, and potentially other hydration phases, in the outer sections of the exposed mortar specimens and consequently increases the porosity of these sections. This additional porosity might be filled with the chloride-containing exposure solution and therefore affect the total chloride content determined with potentiometric titration in the leached sections.

The difference in the maximum total chloride content between the specimens exposed to the NaCl solution and the NaCl+KOH solution for 180 days is about 0.7 wt% of chloride per dried mortar (Fig. 5). To verify whether this difference can be linked to changes in porosity, we made some rough estimates. The detailed calculations are reported as supplementary data to this paper. The free chloride content estimated by filling the porosity with exposure solution is approx. 0.11 wt% Cl per dried mortar. This means that variations in the free chloride content cannot explain the 0.7 wt% difference in total chloride content determined experimentally for the two exposure conditions. If all the portlandite leached out, this would lead to an increase in porosity, and therefore an increase in the free chloride content of only 0.008 wt% dry

mortar. Even if all the cement paste washed out of the mortar, this would only contribute to a chloride content of 0.5 wt% of the fully leached-out mortar. So, potential changes in porosity cannot explain the difference of 0.7 wt% in total chloride content between the specimens exposed to the NaCl solution and the NaCl+KOH solution after 180 days.

The limited potential contribution to the total chloride content of saturating the additional porosity with the exposure solution is also supported by the BSE images presented in Fig. 10, which show that, while chloride exposure led to a considerable increase in porosity, it was only in the outermost 0.50 mm. The difference in chloride content between the specimens exposed to the two solutions, however, is greatest for sections at depths of 1–4 mm, where we do not observe a large difference in porosity. We can therefore conclude that the difference in the maximum chloride content between the specimens exposed to the NaCl solution and the NaCl+KOH solution is not solely due to differences in porosity caused by leaching, but must rather be due to changes in the interactions of the hydration phase assemblage with the two exposure solutions.

4.1.2. Changes in the hydration phase assemblage due to leaching

There are two possible ways the interaction of the hydration phase assemblage with the exposure solution might cause a higher total chloride content: the formation of more chloride-containing phases, such as Friedel's salt or Kuzel's salt, or an increase in the chloride binding of the hydration phases upon moderate leaching, i.e., a decrease in the pH of the pore solution.

Several authors have reported on the effect of pH on the chloride-binding capacity of C-S-H and AFm phases like Friedel's salt and Kuzel's salt in closed equilibrium systems [7,13,15,22,33,62]. In this study, we did not measure the pH in the exposed mortar specimens directly, but a decrease in the measured content of portlandite and potassium does indirectly reflect a decrease in the pH of the pore solution.

4.1.2.1. AFm. In the unaffected mortar at 20 mm depth, monosulphate (e.g., $3\text{CaO}\cdot\text{Al}_2\text{O}_3\cdot\text{CaSO}_4\cdot 12\text{H}_2\text{O}$) was found to be the main AFm phase (Fig. 16). This was in agreement with the GEMS modelling results, which predicted the formation of mainly monosulphate and only small amounts of hemicarbonate in the unexposed binder (for 0.01 L solution added in Fig. 4).

Upon exposure to chlorides, the sulphate ions in the monosulphate

structure can be replaced with chloride ions, as shown by Balonis et al. [7]. For the specimen exposed to NaCl, this resulted in the formation of Friedel's salt ($3\text{CaO}\cdot\text{Al}_2\text{O}_3\cdot\text{CaCl}_2\cdot 10\text{H}_2\text{O}$) at depths where the chloride profile shows the highest total chloride content. In the case of the specimen exposed to the NaCl+KOH solution, Kuzel's salt ($3\text{CaO}\cdot\text{Al}_2\text{O}_3\cdot 0.5\text{CaSO}_4\cdot 0.5\text{CaCl}_2\cdot 11\text{H}_2\text{O}$) formed at depths showing the maximum chloride content (Fig. 17). This results in a Cl/Ca ratio and Cl/Al ratio (Fig. 17 and Fig. 18) of the AFm phase in the case of exposure to NaCl solution that is as much as double as high as for the NaCl+KOH solution at depths of 0–10 mm.

The replacement of sulphate ions with chloride ions in AFm phases is commonly accompanied by the formation of ettringite [7,63], as also predicted by the GEMS model results (see Fig. 4). However, neither the formation of ettringite nor an increase in, e.g., the S/Si ratio of the C-S-H could be determined in this study for the sections in which Friedel's salt or Kuzel's salt were detected (Fig. 16). This might be due to the leaching of the sulphate ions into the exposure solution or the difficulty of detecting ettringite using SEM-EDS [22].

Whether Kuzel's salt or Friedel's salt is formed by the replacement of sulphate ions with chloride ions is commonly related to the chloride concentration in the pore solution. Friedel's salt represents the phase forming at higher chloride concentrations [7,64], as also demonstrated by the GEMS model (Fig. 4). The chloride concentration in the pore solution at a specific depth will depend on the chloride ingress rate. Enhanced leaching in the NaCl mortar seems to lead to a greater chloride ingress depth than in the less leached NaCl+KOH mortar. However, the impact of leaching on the chloride ingress rate will be investigated in more detail in a follow-up study applying a multi-ion transport model.

In addition to the chloride concentration, the hydroxyl (OH^-) concentration in the exposure solution may also play an important role, due to the existence of a solid solution between Friedel's salt and hydroxy-AFm [7,65]. Since the hydroxyl concentration in the NaCl+KOH solution is considerably higher than in the NaCl solution, the binding of chlorides by the AFm phases might be limited due to the competition of chloride with hydroxyl ions for their position in the AFm structure [7]. This would lead to less chloride binding by the AFm phase in the case of exposure to NaCl+KOH than with NaCl, as illustrated in Fig. 18 by the Cl/Al ratios of the AFm phase. Moreover, Hemstad et al. [13] observed an increase in the Cl/Al ratio of the solid solution between monocarbonate and Friedel's salt with decreasing pH. However, as SEM-EDS does not allow the quantification of light elements such as oxygen or hydrogen, or their differentiation from carbonate, we were unable to differentiate between hydroxyl and carbonate AFm.

To investigate the impact of leaching on the amount of chloride-containing AFm formed, we can compare the portlandite profiles (Fig. 7) with the weight loss profiles related to AFm (Fig. 8). The severely leached mortar specimen exposed to NaCl shows a maximum weight loss related to AFm decomposition more than double as high as the less leached specimens exposed to NaCl+KOH. Moreover, the depth of portlandite leaching seems to correspond to the depth at which we observe an increase in the weight loss related to AFm.

The increase in the weight loss related to AFm decomposition in the leached sections could be partially due to changes in the composition of the phases or relative enrichment due to leaching as described in 2.3. However, it has been shown that chloride-containing AFm phases such as Friedel's salt are more stable at a slightly decreased pH [66] leading to the formation of more chloride-AFm due to leaching [13]. This could explain why we observe an increase in the weight loss related to AFm in the sections in which portlandite is leached. It also aligns with the fact that the more leached specimen exposed to NaCl shows higher weight loss related to chloride-containing AFm than the less leached NaCl+KOH specimen.

Hemstad et al. [13] observed that extended leaching led to the decomposition of chloride-containing AFm phases. This is in line with the observed reduction in weight loss related to AFm in the outermost section of the mortar specimens exposed to NaCl.

4.1.2.2. C-S-H. The physical chloride binding by C-S-H is also affected by the pH of the exposure solution. The specimens exposed to the NaCl solution showed a higher Cl/Si ratio for the C-S-H than the specimens exposed to the NaCl+KOH solution (see Fig. 11 and Fig. 18). The only exception of this is the Cl/Si ratio measured at the outermost section of the specimen exposed to NaCl+KOH, which is assumed to be an artefact as explained in chapter 3.6.1.

Chlorides compete with other anions in the pore solution, e.g., hydroxyl ions, for accumulation in the diffuse layer of the C-S-H. With decreasing pH, the concentration of hydroxyl ions is reduced and therefore the accumulation of chloride ions in the diffuse layer may become more favoured than the accumulation of hydroxyl ions [33].

In addition, the Ca/Si ratio of the C-S-H phase can be affected by leaching [34]. This has been reported to have a strong impact on the surface charge of the C-S-H and therefore on the accumulation of cations in the Stern layer and anions like chloride in the diffuse layer of the C-S-H [67–69]. As the Ca/Si ratio of the C-S-H decreases, more silanol groups are deprotonated, which leads to an increase in the negative surface charge density of the C-S-H [67,70]. This can then lead to a higher overcompensation by divalent cations like calcium in the Stern layer, which consequently leads to the accumulation of more chloride ions in the diffuse layer of the C-S-H [20,23,24]. Fig. 18 shows that the Ca/Si ratio of the C-S-H did not change significantly at depths greater than 0.3 mm (see also Fig. 12 and Fig. 13). The Ca/Si ratio of the C-S-H cannot therefore explain the differences in the total chloride profiles and the Cl/Si ratios determined with SEM-EDS between the specimen exposed to NaCl and the specimen exposed to NaCl+KOH down to a depth of 10 mm (see Fig. 11 and Fig. 18).

The de-calcification of the C-S-H in the outermost section (0.03 mm) in the specimen exposed to the NaCl solution, however, seems to have caused the adsorption of alkalis, as reported in literature for de-calcified C-S-H [30,61]. The experimental results in this study show this with the high Na/Si ratio (Fig. 14) and K/Si ratio (Fig. 15) determined in the section at 0.03 mm in the specimen exposed to the NaCl solution.

4.1.3. Impact of changes in the phase composition on the total chloride content

The aim of this section is to illustrate with simplified calculations how the changes in the phase compositions presented in Fig. 18 contribute to the total chloride profiles. Assuming that C-S-H and Friedel's salt are the only chloride-binding phases, we can obtain an estimate of the amount and composition of these phases from the thermodynamic modelling results for exposure to 1 L of NaCl (see Fig. 4). We assume a constant amount of these phases, which is a simplification because these phases can partially decompose near the exposed surface upon advanced leaching. The chloride content of the C-S-H is varied according to the measured Cl/Si molar ratio and the chloride content in the Friedel's salt is varied according to the Cl/Al molar ratio, both as a function of depth below the exposed surface. The ideal Cl/Al ratio of Friedel's salt is 1. If the molar ratio of the chloride-containing AFm deviates from this ideal molar ratio, it should not be called Friedel's salt but rather Kuzel's salt and/or a solid solution between Friedel's salt and a carbonate or hydroxide AFm phase, e.g., monocarbonate. In the following, however, it is referred to as Friedel's salt for the sake of simplicity.

For the GEMS calculations in this study, we used the CSHQ solid solution model [50]. The predicted C-S-H composition contains 8.4 mol Si/mol C-S-H and has a molar mass of 1505 g/mol. The thermodynamic model predicts the formation of 66 g C-S-H per 100 g of unreacted cement, which is equivalent to 16.6 g of C-S-H per 100 g of mortar dried at 105 °C when taking into account the mortar proportioning (Table 2) as well as 26 g of bound water per 100 g cement. This results in a Si content in C-S-H of 0.093 mol/100 g mortar dried at 105 °C¹ If this is

¹ Si content in C-S-H = (16.6 g C-S-H per 100 g mortar dried at 105 °C / 1505 g/mol C-S-H) · 8.4 mol Si/mol C-S-H = 0.093 mol/100 g mortar dried at 105 °C

multiplied by the fitted Cl/Si ratio based on the EDS results and the molar mass of chlorine (35.45 g/mol), we obtain the chloride content in C-S-H as wt% per mortar dried at 105 °C, as illustrated in Fig. 19.

For Friedel's salt (Fs), we assume the ideal chemical composition $3\text{CaO}\cdot\text{Al}_2\text{O}_3\cdot\text{CaCl}_2\cdot 10\text{H}_2\text{O}$ with a molar mass of 561 g/mol. The model predicts the formation of 10 g Fs per 100 g of unreacted cement, or 2.6 g per 100 g of mortar dried at 105 °C. This results in an aluminium content in Fs of 0.0092 mol/100 g mortar dried at 105 °C.² Multiplying this by the fitted Cl/Al molar ratio obtained from EDS and the molar mass of chlorine, we obtain the chloride content in Fs as wt% per mortar dried at 105 °C, as illustrated in Fig. 19.

The amount of chloride found in the pore solution in the outermost section is simulated by assuming that the pore volume is filled with a solution with a chloride concentration similar to the exposure solution. In the above section on porosity, this was calculated to be 0.11 wt% Cl in mortar dried at 105 °C. Deeper into the mortar, the chlorides present in the pore solution were gradually reduced to zero at an ingress depth of 20 mm.

Fig. 19 compares the measured total chloride profiles with the calculated contribution of chlorides in the pore solution, in Friedel's salt, and in C-S-H, as described above. Fig. 20 shows the measured Cl/Al and Cl/Si molar ratios as a function of depth below the exposed surface (see also Fig. 18), as well as fitted curves, which were used for the calculations described above. The curves were fitted so that the measured and calculated total chloride profiles would match both for NaCl exposure and for NaCl+KOH.

The fitted molar ratio curves in Fig. 20 used for the calculations are slightly lower than the measured values. This could be due to an overestimation of the experimentally determined ratios, which is definitely the case for lower chloride contents at greater depths, as mentioned in the respective results section. Moreover, the thermodynamic model might also overestimate the Friedel's salt content slightly, because no correction for the aluminium uptake of the C-S-H was performed, which will lead to lower Cl/Al ratios when fitting the total chloride profiles.

These simplified calculations show that the free chlorides in the pore solution contribute with less than 10% of the maximum total chloride content. C-S-H seems to contribute most to the chloride binding. The chlorides bound by C-S-H stand for almost half of the total chloride content. The remaining 30–40% of the total chloride content is bound in chloride-containing AFm. This is the case, even though the Cl/Si ratio determined is much lower than the Cl/Al ratio (see Fig. 20), because considerably more C-S-H is present in the specimens than AFm.

Based on these calculations, we can conclude that the difference in the total chloride content for NaCl exposure and NaCl+KOH exposure in our findings is due to differences in the chloride uptake in the hydration phases caused by leaching.

4.2. Impact of leaching on the peaking behaviour

After 180 days of exposure, the mortar specimen exposed to the NaCl solution showed a so-called "peaking behaviour", which means that the total chloride content in the outermost section is slightly lower than in the section slightly deeper in (Fig. 5). This peaking of chloride profiles in long-term chloride-exposed concrete has been reported previously [6,30,55].

In specimens not constantly immersed in chloride solution, e.g. concrete structures located in the tidal zone or exposed to de-icing salts, this peaking behaviour is commonly attributed to drying and wetting cycles [1,71,72]. However, it has also been observed in constantly submerged specimens, which are assumed to be fully saturated, as in the case of this study. The peaking behaviour has also been observed in specimens exposed to sea water, but its appearance in specimens

exposed to NaCl solutions shows that other elements present in sea water, such as sulphur or magnesium, are not its sole cause. Instead, leaching of the outermost section and the pH-dependent binding capacity of hydration phases have been proposed as the main reason for the observed peaking behaviour [6,13,30].

Hemstad et al. reported that a drop of the pH below approx. 11 results in the dissolution of chloride-binding hydrate phases, such as Friedel's salt and C-S-H [13]. This corresponds to the reduced weight loss related to the chloride-containing AFm in the outermost section for the specimen exposed to the NaCl solution (Fig. 8). When chloride-containing hydrates are dissolved, the total chloride profile, which is mainly governed by the amount of bound chloride, decreases as well.

In addition to the amount of chloride-containing AFm phases determined by TGA, the SEM-EDS results showed a lower chloride content of the C-S-H (Fig. 11) and AFm phases (Fig. 17) for the outermost sections than for sections slightly deeper in, as summarized in Fig. 18.

The reason for the lower chloride content in the C-S-H in the outermost sections is most likely severe decalcification due to leaching. The calcium is leached out of the specimen during the exposure and cannot therefore compensate for the negative surface charge of the C-S-H by adsorption in the Stern layer. This reduces the accumulation of chloride ions in the diffuse layer and leads to a lower Cl/Si ratio in the outermost section of the C-S-H, as observed with SEM-EDS (Fig. 10).

The decrease in the Cl/Al ratio in the AFm phase in the outermost section is probably due to the presence of carbonates at the exposed surface (see Fig. 10), most likely due to carbonation during sample preparation. Carbonates will result in the formation of monocarbonate ($3\text{CaO}\cdot\text{Al}_2\text{O}_3\cdot\text{CaCO}_3\cdot 11\text{H}_2\text{O}$), which is more stable upon leaching than Friedel's salt as can be seen from the thermodynamic model (Fig. 4), and will lead to an overall reduction in the Cl/Al ratio detected with SEM-EDS.

In summary, the decomposition of chloride-containing AFm phases and the decrease in the chloride content in AFm and C-S-H in the outermost sections can explain the observed peaking behaviour in the near-surface region in the total chloride profile.

4.3. Impact on service life modelling and performance testing

As mentioned in the introduction, chloride profiles are commonly used to predict chloride ingress in concrete over time. Typically, the chloride profiles are fitted using a least-mean-square method with the error function solution for Fick's 2nd law of diffusion, and an apparent diffusion coefficient and a surface concentration are obtained as fitting parameters [1,73]. Fig. 21 shows the fitted error function solution of Fick's 2nd law for the chloride profiles measured, as well as the fitted apparent diffusion coefficient and surface concentration.

Due to the so-called peaking behaviour (see Section 4.2), the near-surface points in the chloride profile often do not fit the error function solution and are therefore omitted. The assumption of a constant surface concentration, C_s , in the models used by *fib* and ISO [1,73] is questionable. The chloride profiles for NaCl exposure in Fig. 5 show that the surface concentration nearly doubles between 90 and 180 days of exposure, which demonstrates that the surface concentration is not necessarily constant in time. However, in the case of NaCl+KOH exposure, we do not observe significant change in the surface concentration between 90 and 180 days of exposure. We attribute the variation in the surface concentrations with time to continuous "moderate" leaching of the outer sections of the mortar, which causes a gradual increase in the chloride-binding capacity of the cement paste and a gradually deeper location for the maximum chloride concentration over time. Models using the error function solution of Fick's 2nd law should take account of this time-dependent surface concentration.

The *fib* model code is able to account for apparent changes in the diffusive properties of the concrete with time by using a so-called ageing exponent for the diffusion coefficient [1]. By comparing the fitted

² Al content in Fs = (2.6 g Fs per 100 g mortar dried at 105 °C / 561 g/mol Fs) · 2 mol Al/mol Fs = 0.0092 mol/100 g mortar dried at 105 °C

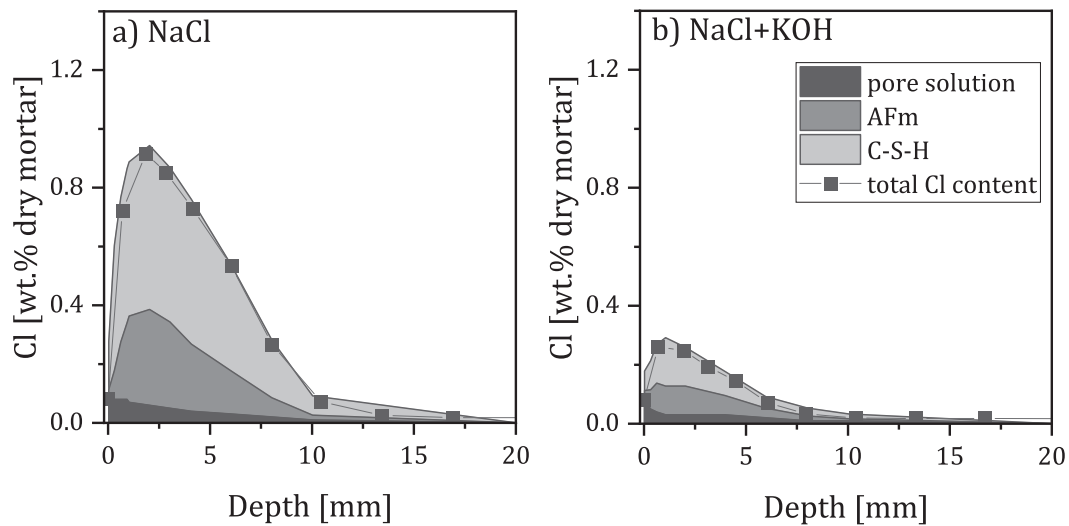


Fig. 19. Measured total chloride content (symbols), and calculated chloride content in Friedel's salt (Fs), C-S-H, and pore solution (cumulative area plots) in wt% of mortar dried at 105 °C as a function of depth below the exposed surfaces of the mortar specimens exposed to a) the NaCl solution or b) the NaCl+KOH solution for 180 days.

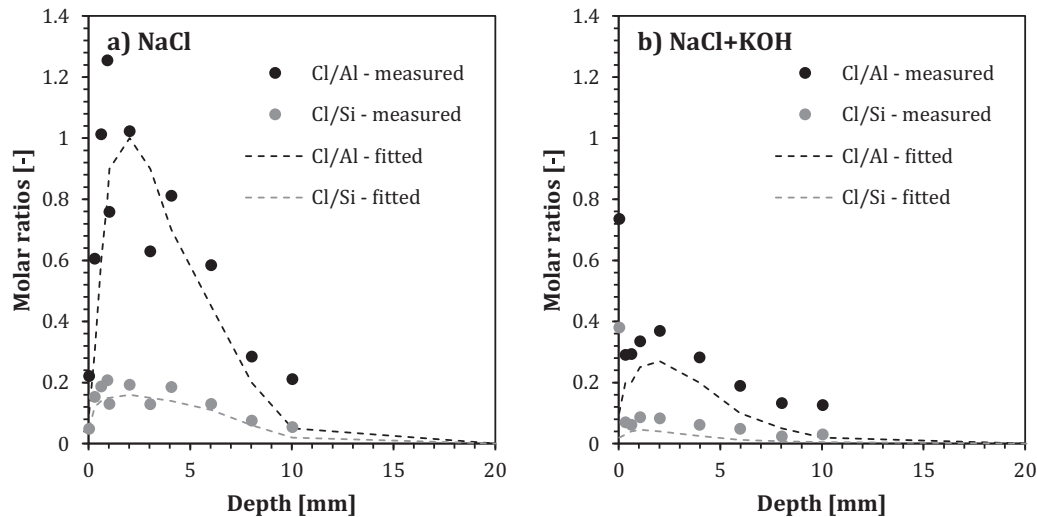


Fig. 20. Measured (symbols) and fitted (lines) molar ratios of Cl/Al and Cl/Si as a function of depth below the exposed surfaces of the mortar specimens exposed to a) the NaCl solution or b) the NaCl+KOH solution for 180 days.

apparent diffusion coefficients and surface concentrations in Fig. 21, we demonstrate that the evolution over time of the diffusion coefficient and surface concentration are exposure-dependent. We will look further into this dependency of the diffusion coefficient on leaching in a follow-up study with the help of a multi-ion transport model.

Recently, it has been proposed to model chloride ingress over time using a so-called “square root method” [74,75]. The model relies on a linear relationship between the ingress depth of a selected “reference” total chloride content and the square root of the exposure time. By following one given concentration, the impact of pH-dependent binding capacity is limited. Furthermore, if one selects a “reference” total chloride content, which is not only slightly affected by leaching, one would purely focus on the ingress rate. In our case, a potential reference concentration could for example be a content of 0.1 wt% mortar (see Fig. 5). In the light of our results, the rather simple square root method appears to be a promising engineering approach for chloride ingress prediction.

The findings of this study also have an impact on performance testing

of the chloride ingress resistance of concrete such as [35,76–79]. Performance testing should be valid (relevant) and reliable (repeatable). In order to be relevant, the leaching conditions during the performance testing should represent the conditions during exposure. In the laboratory, the leaching conditions can be relatively mild, because concrete is exposed to a limited volume of chloride solution, e.g., in a container or by ponding. Whereas in the case of exposure to the sea, for example, the concrete is exposed to an unlimited reservoir and therefore to harsh leaching. Underrepresenting the leaching conditions during performance testing might lead to non-conservative and therefore not relevant estimates of the chloride ingress resistance of the concrete. In order for the performance tests to be repeatable, leaching needs to be clearly described and documented, e.g., by specifying the exposed surface area per litre exposure solution and specifying the frequency of renewal of the exposure solution. This also illustrates the importance of testing the actual concrete in the actual environment and supports the suggestion of the establishment of a “birth certificates” as suggested several decades ago by Rostam [80] and recently in a *fib* Bulletin [81].

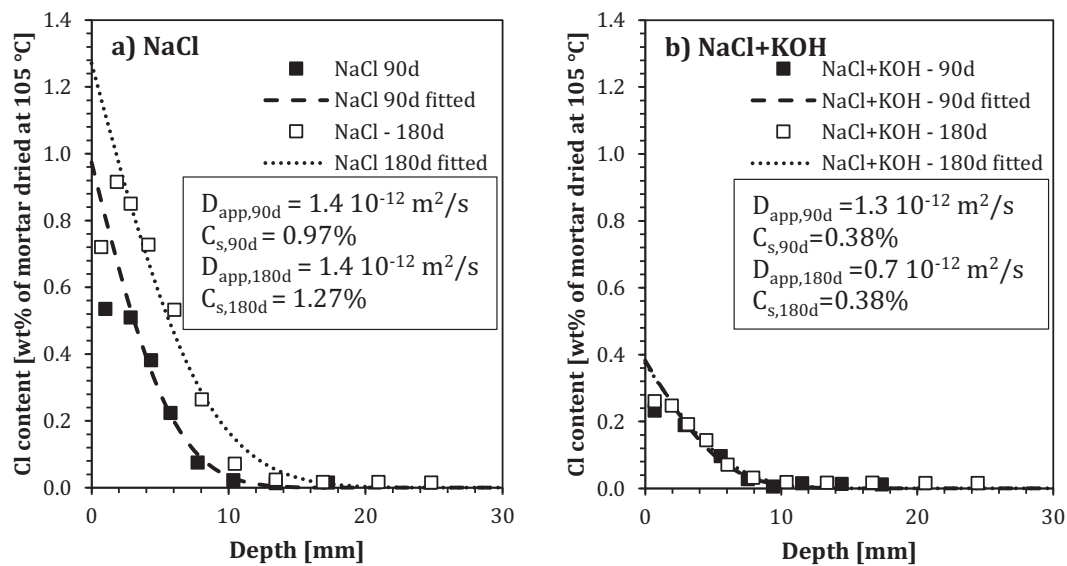


Fig. 21. Fitted error function solution of Fick's 2nd law for the chloride profiles measured for a) exposure to the NaCl and b) the NaCl+KOH solution. The fitted diffusion coefficient and surface concentration are listed. We have omitted the outermost points of the chloride profiles during fitting.

5. Outlook and further research

In this study, both exposure solutions used have the same chloride concentration. Potential differences in the chloride concentration in the pore solution at various depths, causing, e.g., the formation of Friedel's salt instead of Kuzel's salt, can therefore only be related to differences in the chloride ingress rate between the two exposure solutions.

Leaching has a strong impact on the chloride ingress rate, because electroneutrality needs to be maintained according to the Poisson-Nernst-Planck equation [72]. The amount and charge of ions that leach from the specimen into the exposure solution therefore affect the amount and charge of the ions that are able to penetrate from the exposure solution into the specimen.

Since electroneutrality needs to be maintained, the ingress of chloride anions is commonly accompanied by leaching of hydroxyl anions from the specimen into the exposure solution, which is the case for exposure to the NaCl solution. In the case of the specimen that was exposed to the NaCl+KOH solution, leaching of hydroxyl ions was limited due to the high hydroxyl concentration of the exposure solution. Consequently, sodium cations were forced to penetrate the specimens together with the chloride anions to maintain the electroneutrality of the pore solution. Note that for the NaCl exposure, the sodium cations do not follow the chloride ions, because hardly any ingress of sodium cations is observed (Figs. 9 a) and 18). The assumption that the sodium ingress is related to the chloride ingress in the case of exposure to the NaCl+KOH solution is supported by the fact that there is almost no difference in the sodium profiles between 90 and 180 days (Fig. 9 a), which is also the case for the chloride profiles of these specimens (Fig. 5).

These complex transport mechanisms will be investigated in more detail in another part of this project by applying a multi-ion transport model to simulate the transport of chlorides into the specimens exposed to the two different leaching conditions applied in this study.

6. Conclusions

Exposure of mortar specimens for up to 180 days to a 3% NaCl solution was able to provoke intense leaching, whereas exposure to 3% NaCl+KOH led to limited leaching. The extent of leaching strongly affected the chloride ingress profiles. After 180 days of exposure, the most leached specimens exposed to the NaCl solution showed almost three times higher maximum total chloride content and considerably

higher chloride ingress depth than the less leached specimens exposed to the NaCl+KOH solution.

The purpose of this research was to explain why the chloride ingress profiles are that different for the two exposure solutions even though the solutions have the same chloride concentration.

Total chloride profiles are governed by the interaction with hydration phases. Our calculations show that porosity contributes less than 10% of the maximum total chloride content and thereby only plays a minor role. The Cl-uptake in C-S-H on the other hand accounts for about 50% and chloride binding by AFm contributes 40%. Their Cl-uptake is affected by leaching:

- The Cl/Si molar ratio of the C-S-H was higher in the case of the NaCl exposure solution than for the NaCl+KOH exposure solution. This is probably due to the reduced competition with hydroxyl anions for accumulation in the diffuse layer in the more leached NaCl specimen.
- The chloride-binding AFm phase observed for the NaCl exposure was Friedel's salt at the maximum total chloride content, whereas Kuzel's salt was observed in the case of NaCl+KOH, resulting in a Cl/Al molar ratio for the AFm in the NaCl exposure that was twice as high as in the NaCl+KOH exposure.

The maximum total chloride content in the more leached NaCl mortar is three times higher than in the less leached NaCl+KOH exposed mortar, which is due to the enhanced binding capacity of the C-S-H and AFm upon moderate leaching. In the severely leached outermost section of the NaCl exposed specimen, the chloride binding is reduced due to decalcification of the C-S-H and probably carbonation of the AFm. Moreover, some of the chloride-containing AFm phases decomposed in the outermost section of the specimen exposed to the NaCl solution. This shows that the pH-dependent chloride-binding capacity determines the shape of total chloride profiles, including the so-called peaking behaviour in the near-surface region in long-term exposed specimens.

The chloride ingress rate is also clearly affected by leaching. This will be further investigated in a follow-up study with the help of a multi-ion transport model.

CRedit authorship contribution statement

Alisa Machner: conceptualization, methodology, software, formal analysis, investigation, writing – original draft, review & editing,

visualization, supervision, project administration.

Marie H. Bjørndal: investigation, writing – review & editing.

Harald Justnes: conceptualization, methodology, writing – review & editing.

Lucija Hanžič: methodology, investigation, writing – original draft, review & editing, visualization.

Aljoša Šajna: methodology, investigation, writing – review & editing.

Yushan Gu: methodology, writing – review & editing.

Benoit Bary: methodology, writing – review & editing.

Mohsen Ben Haha: methodology, writing – review & editing, funding acquisition, project administration.

Mette R. Geiker: conceptualization, methodology, writing – original draft, review & editing, visualization.

Klaartje De Weerd: conceptualization, methodology, software, formal analysis, writing – original draft, review & editing, visualization, supervision, funding acquisition, project administration.

Declaration of competing interest

The authors declare hereby that for none of us there exists a conflict of interest.

Acknowledgements

The authors would like to thank EnDurCrete project partner Rosa Marie Carreras Lample from Acciona for preparing the mortar specimens for this study. We would also like to thank Sebastijan Robič from ZAG for help with the specimen exposure and profile grinding, Siri Hofstad Trapnes from SINTEF, and Tone H. Nilsen and Oda Tjetland from NTNU for their help with the chloride titration and TGA measurements, Syverin Lierhagen from NTNU for the ICP-MS analyses, and Ulla Hjorth Jakobsen and her team from DTI for the preparation of the polished sections for SEM-EDS.

This project has received funding from the European Union's Horizon 2020 research and innovation programme under grant agreement No 760639 and this publication reflects only the authors' view and the Commission is not responsible for any use that may be made of the information it contains.



Appendix A. Supplementary data

Supplementary data to this article can be found online at <https://doi.org/10.1016/j.cemconres.2021.106691>.

References

- [1] International Federation for Structural Concrete (fib), fib Bulletin 34: Model Code for Service Life Design: Model code prepared by Task Group 5.6, fib, Lausanne, 2006.
- [2] A. Fick, Über diffusion, Ann. Phys. 170 (1855) 59–86.
- [3] H. Justnes, M.R. Geiker, A critical view on service life predictions based on chloride induced corrosion, in: Proceedings of the 2nd International Conference on "Microdurability" (Microstructure Related Durability of Cementitious Composites), Amsterdam, the Netherlands, 2012, pp. 37–50.
- [4] M.R. Geiker, H. Justnes, Prediction of chloride induced corrosion for service life modelling, in: 1st International Congress on Durability of Concrete (ICDC), 2012.
- [5] K.De Weerd, S.G. Ytterdal, M.R. Geiker, On the impact of phase changes on chloride profiles in concrete, in: Proceedings of the XXII Nordic Concrete Research Symposia, Norsk Betongforening, 2014, pp. 369–372.
- [6] K. De Weerd, D. Orsáková, A.C.A. Müller, C.K. Larsen, B. Pedersen, M.R. Geiker, Towards the understanding of chloride profiles in marine exposed concrete, impact of leaching and moisture content, Constr. Build. Mater. 120 (2016) 418–431.
- [7] M. Balonis, B. Lothenbach, G. Le Saout, F.P. Glasser, Impact of chloride on the mineralogy of hydrated Portland cement systems, Cem. Concr. Res. 40 (2010) 1009–1022.
- [8] U.A. Birmin-Yauri, F.P. Glasser, Friedel's salt, Ca₂Al(OH)₆(Cl, OH)·2H₂O: its solid solutions and their role in chloride binding, Cem. Concr. Res. 28 (1998) 1713–1723.
- [9] F.P. Glasser, A. Kindness, S.A. Stronach, Stability and solubility relationships in AFm phases: Part I. Chloride, sulfate and hydroxide, Cem Concr Res 29 (1999) 861–866.
- [10] H. Pöllmann, Solid solutions of complex calcium aluminate hydrates containing Cl⁻, OH⁻ and CO₃²⁻ anions, in: Proceedings of the 8th International Congress on the Chemistry of Cement, Rio de Janeiro, 1986, pp. 300–306.
- [11] H. Pöllmann, Mischkristallbildung in den Systemen 3CaO·Al₂O₃·CaCl₂·10H₂O – 3CaO·Al₂O₃·CaCO₃·11H₂O und 3CaO·Al₂O₃·CaCl₂·10H₂O – 3CaO·Al₂O₃·Ca(OH)₂·12H₂O, 1980.
- [12] M.Y. Hobbs, Solubilities and ion exchange properties of solid solutions between the OH, Cl and CO₃ end members of the monocalcium aluminate hydrates, 2001. PhD Thesis, Canada.
- [13] P. Hemstad, A. Machner, K. De Weerd, The effect of artificial leaching with HCl on chloride binding in ordinary Portland cement paste, Cem. Concr. Res. 130 (2020), 105976.
- [14] C. Shi, Q. Yuan, F. He, X. Hu, Transport and interactions of chlorides in cement-based materials, 1st ed., CRC Press Taylor & Francis Group, 2020.
- [15] K. De Weerd, A. Colombo, L. Coppola, H. Justnes, M.R. Geiker, Impact of the associated cation on chloride binding of Portland cement paste, Cem. Concr. Res. 68 (2015) 196–202.
- [16] C. Arya, N.R. Buenfeld, J.B. Newman, Factors influencing chloride-binding in concrete, Cem. Concr. Res. 20 (1990) 291–300.
- [17] Z. Shi, M.R. Geiker, K. De Weerd, T.A. Østnor, B. Lothenbach, F. Winnefeld, J. Skibsted, Role of calcium on chloride binding in hydrated Portland cement–metakaolin–limestone blends, Cem. Concr. Res. 95 (2017) 205–216.
- [18] A. Delagrave, J. Marchand, J.-P. Ollivier, S. Julien, K. Hazrati, Chloride binding capacity of various hydrated cement paste systems, Adv. Cem. Based Mater. 6 (1997) 28–35.
- [19] Q. Zhu, L. Jiang, Y. Chen, J. Xu, L. Mo, Effect of chloride salt type on chloride binding behavior of concrete, Constr. Build. Mater. 37 (2012) 512–517.
- [20] O. Wowra, M.J. Setzer, Sorption of chlorides on hydrated cement and C3S pastes, in: M.J. Setzer, R. Auberg (Eds.), Frost Resistance of Concrete, E & FN Spon, London, 1997, pp. 147–153.
- [21] A. Machner, M. Zajac, M. Ben Haha, K.O. Kjellsen, M.R. Geiker, K. De Weerd, Chloride-binding capacity of hydrotalcite in cement pastes containing dolomite and metakaolin, Cem Concr Res 107 (2018) 163–181.
- [22] K. De Weerd, D. Orsáková, M.R. Geiker, The impact of sulphate and magnesium on chloride binding in Portland cement paste, Cem. Concr. Res. 65 (2014) 30–40.
- [23] C. Labbez, A. Nonat, I. Pochard, B.G. Jönsson, Experimental and theoretical evidence of overcharging of calcium silicate hydrate, J. Colloid Interface Sci. 309 (2007) 303–307.
- [24] G. Plusquellec, A. Nonat, Interactions between calcium silicate hydrate (C-S-H) and calcium chloride, bromide and nitrate, Cem. Concr. Res. 90 (2016) 89–96.
- [25] H. Justnes, A review of chloride binding in cementitious systems, Nordic Concr. Res. 21 (1998) 48–63.
- [26] H. Justnes, K. De Weerd, M.R. Geiker, Chloride binding in concrete exposed to sea water and salt solutions, in: Z.J. Li, C.W. Miao, O.E. Gjörv, W. Sun, K. Sakai, N. Banthia (Eds.), Seventh International Conference on Concrete under Severe Conditions (CONSEC13) Nanjing, China, 23–25 September 2013, RILEM Proceedings PRO, 2013, pp. 653–665.
- [27] H. Justnes, E. Rodum, Case studies of thaumasite formation, in: Proceedings of the Seventh CANMET/ACI International Conference on Durability of Concrete, Montreal, 2006, pp. 521–537.
- [28] C. Jones, S. Ramanathan, P. Suraneni, W.M. Hale, Calcium oxychloride: a critical review of the literature surrounding the formation, deterioration, testing procedures, and recommended mitigation techniques, Cem. Concr. Compos. 113 (2020), 103663.
- [29] P. Suraneni, J.V. Azad, B.O. Isgor, J.W. Weiss, Calcium oxychloride formation in pastes containing supplementary cementitious materials: thoughts on the role of cement and supplementary cementitious materials reactivity, RILEM Tech. Lett. 1 (2016) 24–30.
- [30] K. De Weerd, B. Lothenbach, M.R. Geiker, Comparing chloride ingress from seawater and NaCl solution in Portland cement mortar, Cem. Concr. Res. 115 (2019) 80–89.
- [31] A. Machner, P. Hemstad, K. De Weerd, Towards the understanding of the pH dependency of the chloride binding of Portland cement pastes, Nordic Concr. Res. 58 (2018) 143–162.
- [32] Z. Shi, M.R. Geiker, B. Lothenbach, K. De Weerd, S.F. Garzón, K. Enemark-Rasmussen, J. Skibsted, Friedel's salt profiles from thermogravimetric analysis and thermodynamic modelling of Portland cement-based mortars exposed to sodium chloride solution, Cem. Concr. Compos. 78 (2017) 73–83.

- [33] J. Tritthart, Chloride binding in cement II. The influence of the hydroxide concentration in the pore solution of hardened cement paste on chloride binding, *Cem Concr Res* 19 (1989) 683–691.
- [34] I. Pointeau, P. Reiller, N. Macé, C. Landesman, N. Coreau, Measurement and modeling of the surface potential evolution of hydrated cement pastes as a function of degradation, *J. Colloid Interface Sci.* 300 (2006) 33–44.
- [35] EN 12390-11, Testing hardened concrete – Part 11: Determination of the chloride resistance of concrete, unidirectional diffusion, CEN, European Committee for Standardization, Brussels, 2015.
- [36] A. Machner, M.H. Bjørndal, A. Sajna, N. Mikanovic, K. De Weerdt, Impact of leaching on chloride ingress profiles in concrete 55, *Materials and Structures*, 2022, 8. In press.
- [37] EN 197-5, Cement - Part 5: Portland-composite cement CEM II/C-M and Composite cement CEM VI: German version EN 197-5:2021, European Committee for Standardization, Brussels, 2021.
- [38] EN 197-1 - new version under development, Cement, Part I: Composition, specifications and conformity criteria for common cements. CEN, European Committee for Standardization, Brussels, not issued yet.
- [39] EN 12390-2, Testing hardened concrete - Part 2: Making and curing specimens for strength tests, CEN, European Committee for Standardization, Brussels, 2001.
- [40] EN 206, Concrete – Specification, performance, production and conformity, European Committee for Standardization, Brussels, 2017.
- [41] B. Lothenbach, P.T. Durdziński, K. De Weerdt, Thermogravimetric analysis, in: K. L. Scrivener, R. Snellings, B. Lothenbach (Eds.), *A Practical Guide to Microstructural Analysis of Cementitious Materials*, CRC Press Taylor & Francis Group, Boca Raton, 2016, pp. 177–211.
- [42] A. Machner, M. Zajac, M. Ben Haha, K.O. Kjellsen, M.R. Geiker, K. De weerd, stability of the hydrate phase assemblage in Portland composite cements containing dolomite and metakaolin after leaching, carbonation, and chloride exposure, *Cem. Concr. Compos.* 89 (2018) 89–106.
- [43] H.F.W. Taylor, *Cement Chemistry*, 2nd ed., Telford, London, 1997.
- [44] B. Lothenbach, F. Winnefeld, Thermodynamic modelling of the hydration of Portland cement, *Cem. Concr. Res.* 36 (2006) 209–226.
- [45] D.A. Kulik, GEM-Selektor v.3.3.
- [46] T. Wagner, D.A. Kulik, F.F. Hingerl, S.V. Dmytrieva, GEM-selektor geochemical modeling package: TSoMod library and data interface for multicomponent phase models, *Can. Mineral.* 50 (2012) 1173–1195.
- [47] D.A. Kulik, T. Wagner, S.V. Dmytrieva, G. Kosakowski, F.F. Hingerl, K. V. Chudnenko, U.R. Berner, GEM-selektor geochemical modeling package: revised algorithm and GEMS3K numerical kernel for coupled simulation codes, *Comput. Geosci.* 17 (2013) 1–24.
- [48] Thermodynamic database, provided by EMPA, available at: <https://www.empa.ch/web/s308/thermodynamic-data>.
- [49] B. Lothenbach, D.A. Kulik, T. Matschei, M. Balonis, L. Baquerizo, B. Dilnesa, G. D. Miron, R.J. Myers, Cemdata18: a chemical thermodynamic database for hydrated Portland cements and alkali-activated materials, *Cem. Concr. Res.* 115 (2019) 472–506.
- [50] D.A. Kulik, Improving the structural consistency of C-S-H solid solution thermodynamic models, *Cem. Concr. Res.* 41 (2011) 477–495.
- [51] R. Loser, B. Lothenbach, A. Leemann, M. Tuchschnid, Chloride resistance of concrete and its binding capacity – comparison between experimental results and thermodynamic modeling, *Cem. Concr. Compos.* 32 (2010) 34–42.
- [52] K. De Weerdt, H. Justnes, M.R. Geiker, Changes in the phase assemblage of concrete exposed to sea water, *Cem. Concr. Compos.* 47 (2014) 53–63.
- [53] EnDurCrete, D2.4 Report on hydration study: WP2, 2019.
- [54] EnDurCrete, D4.1 Report on modelling the phase assemblage of novel binders: WP4, 2019.
- [55] C. Andrade, M.A. Climent, G. de Vera, Procedure for calculating the chloride diffusion coefficient and surface concentration from a profile having a maximum beyond the concrete surface, *Mater. Struct.* 48 (2015) 863–869.
- [56] U.H. Jakobsen, K. De Weerdt, M.R. Geiker, Elemental zonation in marine concrete, *Cem. Concr. Res.* 85 (2016) 12–27.
- [57] A.Baba Ahmadi, A. Machner, W. Kunther, P. Hemstad, K.De Weerdt, Chloride binding in Portland composite cements containing metakaolin and silica fume, submitted for publication to *Cement and Concrete Research*, 2021.
- [58] J. Eikenberg, On the Problem of Silica Solubility at High pH: PSI-Bericht Nr. 74, Würenlingen and Villingen, 1990.
- [59] E.J. Reardon, Problems and approaches to the prediction of the chemical composition in cement/water systems, *Waste Manag.* 12 (1992) 221–239.
- [60] B. Lagerblad, Leaching Performance of Concrete Based on Studies of Samples from Old Concrete Constructions: Technical Report TR-01-27, Bromma, Sweden, 2001.
- [61] E. L'Hôpital, B. Lothenbach, K. Scrivener, D.A. Kulik, Alkali uptake in calcium alumina silicate hydrate (C-A-S-H), *Cem Concr Res* 85 (2016) 122–136.
- [62] H. Zibara, Binding of external chlorides by cement pastes, PhD Thesis, University of Toronto, 2001.
- [63] F. Althoezy, Compressive strength reduction of cement pastes exposed to sodium chloride solutions: secondary ettringite formation, *Constr. Build. Mater.* 299 (2021).
- [64] M. Balonis, Thermodynamic modelling of temperature effects on the mineralogy of Portland cement systems containing chloride, *Cem. Concr. Res.* 120 (2019) 66–76.
- [65] T. Matschei, B. Lothenbach, F.P. Glasser, The AFm phase in Portland cement, *Cem. Concr. Res.* 37 (2007) 118–130.
- [66] M.H. Roberts, Effect of calcium chloride on the durability of pre-tensioned wire in prestressed concrete, *Mag. Concr. Res.* 14 (1962) 143–154.
- [67] Y. Zhou, D. Hou, J. Jiang, L. Liu, W. She, J. Yu, Experimental and molecular dynamics studies on the transport and adsorption of chloride ions in the nano-pores of calcium silicate phase: the influence of calcium to silicate ratios, *Microporous Mesoporous Mater.* 255 (2018) 23–35.
- [68] J.J. Beaudoin, V.S. Ramachandran, R.F. Feldman, Interaction of chloride and C-S-H, *Cem. Concr. Res.* 20 (1990) 875–883.
- [69] S. Yoon, J. Ha, S.R. Chae, D.A. Kilcoyne, P.J.M. Monteiro, X-ray spectromicroscopic study of interactions between NaCl and calcium silicate hydrates, *Mag. Concr. Res.* 66 (2014) 141–149.
- [70] Jérémy Haas, Etude expérimentale et modélisation thermodynamique du système CaO-SiO₂-(Al₂O₃)-H₂O, 2012. PhD thesis, France.
- [71] L. Bertolini, B. Elsener, P. Pedferri, R.B. Polder, Corrosion of Steel in Concrete: Prevention, Diagnosis, Repair, Wiley, Weinheim, 2003. PhD thesis, France.
- [72] T. Luping, L.-O. Nilsson, P.A.M. Basheer, Resistance of Concrete to Chloride Ingress, 1st ed., Spon Press, London and New York, 2012.
- [73] ISO 16204, Durability - Service Life Design of Concret Structures, International Organization for Standards, Geneva, Switzerland, 2012.
- [74] S. Fjendbo, H.E. Sørensen, K. De Weerdt, M.R. Geiker, The square root method for chloride ingress prediction - applicability and limitations, *Mater. Struct.* 54 (2021).
- [75] S.L. Poulsen, H.E. Sørensen, Chloride ingress in old Danish bridges, in: 2nd International Congress on Durability of Concrete (ICDC), 2014.
- [76] EN 13396, Products and systems for the protection and repair of concrete structures, in: Test methods. Measurement of chloride ion ingress, CEN, European Committee for Standardization, Brussels, 2004.
- [77] ASTM C1543-10a, Standard Test Method for Determining the Penetration of Chloride Ion into Concrete by Ponding, ASTM International, West Conshohocken, PA, United States, 2010.
- [78] NT BUILD 443, Concrete, hardened: Accelerated chloride penetration. Nordtest, Nordtest, Espoo, Finland, 1995.
- [79] ASTM C1556-11a, Standard Test Method for Determining the Apparent Chloride Diffusion Coefficient of Cementitious Mixtures by Bulk Diffusion, ASTM International, West Conshohocken, PA, United States, 2016.
- [80] S. Rostam, Performance-based design of structures for the future, in: A. Golay (Ed.), IABSE Symposium “Structures for the Future – The Search for Quality”, 1999.
- [81] International Federation for Structural Concrete (fib), fib Bulletin 93: Birth Certificate and Through-life Management Documentation. Technical Report, fib, Lausanne, 2020.